Molecular dynamics simulation of nanocomposite materials

by

Yin Yani

A dissertation submitted to the graduate faculty

in partial fulfillment of the requirements for the degree of

DOCTOR OF PHILOSOPHY

Major: Chemical Engineering

Program of Study Committee:

Monica H. Lamm, Major Professor
Mark S. Gordon
R. Dennis Vigil
Eric W. Cochran
Zhiqun Lin

Iowa State University

Ames, Iowa

2009

TABLE OF CONTENTS

ABSTRACT

Mixed-matrix materials are a class of nanocomposites that contain a rigid, inorganic chemical species within a polymer matrix. The addition of the inorganic species necessarily affects the structures and thermal properties of the original polymeric material. In this thesis, mixed-matrix materials containing polymer and polyhedral oligomeric silsesquioxanes (POSS) are studied with molecular dynamics simulation to provide molecular insight about the property enhancements observed experimentally for this class of material.

Three different polymer matrices are considered: glassy polymer (polyimide, PI), flexible polymer (polydimethylsiloxane, PDMS), and a copolymer composed of the glassy and flexible segments. Two different POSS, octahydrido silsesquioxane (OHS) and octaaminophenyl silsesquioxane (OAPS) are studied to observe the effect of different functionalization of POSS in the nanocomposite material. The glass transition temperature of the PI/OAPS, PDMS/OAPS, and PI-PDMS/OAPS blends increases with the incorporation of OAPS. A decrease in the glass transition temperature is shown for the model of PI/OHS blends.

Although the results from the atomistic simulations provide molecular insight about thermal property enhancements afforded by POSS-based additives, there is a limitation of the system size and the time scale being used for such macromolecular system in the atomistic simulation. To overcome this, a coarse-grained (CG) model has been shown to have the capability of eliminating the unimportant degrees of freedom in the atomistic simulation. CG model treats a collection of atoms as a coarse-grained site, and therefore larger system can then be studied at longer time scales. In this work, the CG

model for OHS molecule is obtained by using a force-matching method. The CG model is validated by comparing the OHS structural properties obtained from the CG-MD simulation to the one obtained from the atomistic MD simulation.

CHAPTER 1

1.1 Introduction

Membranes have been widely used in gas separation applications, such as for hydrogen purification, air purification, and natural gas processing. Membranes were first used for gas separation by J. K. Mitchell of Philadelphia in 1831 [1]. He observed that natural rubber balloons, filled with different gas compositions, blew up with different velocities at atmospheric conditions. His experiments showed that carbon dioxide had the fastest permeation velocities compared to hydrogen and air. The rubber film was able to absorb carbon dioxide to a larger degree compared to the other two gases, and therefore, the balloon expanded and porosity was induced in the solid rubber sample which enabled the carbon dioxide molecules to penetrate [1].

The most widely used membranes in industry are made from polymers [2], [3], [4]. Polymeric membranes are cost effective, easy to process, and have good gas transport properties. The main drawback for this type of membrane is the inability to withstand elevated temperatures. For example, polymer membranes cannot be used to produce gases of high purity at elevated process temperatures, because the increased mobility of the polymer chains at high temperatures result in a poor selectivity for the membrane.

Other types of membranes that have been used for gas separation are inorganic membranes. This type of membrane has good permeabilities and selectivities to gases at elevated temperature. However, inorganic membranes are difficult to process and less cost effective compared to polymeric membranes. Because many new applications have high performance expectations for membrane materials, such as thermal stability for

elevated temperature applications, and solvent stability [5], a lot of effort has been put into developing another type of membrane, known as mixed-matrix membranes [6].

Mixed-matrix membranes incorporate an inorganic filler within the polymeric matrix. These membranes combine the thermal stability, rigidity and high selectivity of inorganic fillers with the flexibility, and processability of polymeric materials. The rigid inorganic filler can reduce the mobility of the polymer chains and therefore improve the membrane's selectivity at elevated temperature. However, if a very high loading of the inorganic fillers is used, the polymer chains can become brittle which may lead to the reduction in the permeability of the membrane. Therefore, the loading of the fillers should be optimized to produce a robust mixed-matrix membrane for gas separation.

The possible diffusive pathways of gas transport through a mixed-matrix membrane can be: (i) within the polymer matrix, (ii) within the inorganic filler, and (iii) within the interphase gaps. An understanding of how a polymer interacts with the inorganic fillers is important to be able to minimize the interphase gaps of the mixed-matrix materials. A poor contact between polymer and inorganic filler may lead to an additional nonselective pathway for gas transport.

One approach to improve the contact between polymers and inorganic fillers is to modify the surface of the fillers with organic functional groups to increase its compatibility with the polymer matrix. Polyhedral oligomeric silsesquioxanes (POSS) are one example of the inorganic fillers that have been widely studied for this purpose. POSS is a cage structure consisting of silicon and oxygen atoms. It has a chemical composition of $(RSiO_{1.5})_n$ (n = 4, 6, 8, 10…) with R as an organic functional group. The most common

POSS studied is the octasilsesquioxane (n = 8), which has a cube-shaped of Si_8O_{12} cage with organic groups R at each corner.

1.2 Research Objectives

The overall objective of this project is to analyze the effect that incorporation of POSS within a polymer matrix has on the thermal properties by using molecular dynamics simulation. This molecular-based insight will then be useful to design a robust mixed matrix membrane for hydrogen gas separation. This study will consider mixed matrix materials with three different polymer matrices: glassy polymer (polyimide, 6FDA-MDA), flexible polymer (polydimethylsiloxane, PDMS), and a copolymer composed of glassy and flexible monomers (6FDA-MDA-PDMS). Polyimide was chosen due to its ability to withstand an elevated temperature. In addition, this polymer has been a well-characterized membrane polymer for use in gas separation [7], [8]. PDMS was chosen due to its flexibility. It has a higher permeability compared to polyimide and is not expected to be highly selective unless it is copolymerized with polyimide. Therefore, the last type of polymer to consider in this project is a copolymer composed of polyimide and PDMS.

This work will focus on using T_8 (polyhedral octamer) POSS as the inorganic filler. Even though POSS has been extensively studied as a filler to modify the mechanical and thermal properties of polymers, there are still very few reports in the literature [9], [10] of POSS being used in membrane applications. The ability of POSS to increase the strength and heat resistance when incorporated into nearly all polymers makes it possible to improve membrane properties, especially for hydrogen gas separation applications that require a very high operating temperature.

Our fist study will consider polyimide (PI) as the polymer matrix and two different types of POSS (octahydrido and octaaminophenyl silsesquioxanes) as the fillers. Two different POSS are considered to observe the effect of different functionalization of POSS in the mixed matrix material. There have been quite a lot of studies done experimentally [11], [12], [13] for POSS-polyimide material, however, none was found in the literature for the molecular simulation study of this material. Therefore, the results from this study will be useful for comparison to the experimental studies that have been done.

The second study will consider PDMS polymer and PI-PDMS copolymer as the polymer matrices and octaaminophenyl silsesquioxane (OAPS) as the filler. Only one type of POSS is considered here, because of the incompatibility of octahydrido POSS to PI found from the first study. The Striolo group [14], [15] has done molecular simulation studies of PDMS-POSS material. However, none of their studies have used the octaaminophenyl POSS. In addition to that, there are still no reports either in experiment or simulation works in the literature about the study of poly(imide siloxane)-POSS material.

The third study will consider a coarse-grained model of the octahydrido silsesquioxane (OHS). The force-matching method which was derived by Izvekov *et al.* [16] and implemented by Pranami and coworkers [17] will be applied here. This method will eliminate the unimportant degrees of freedom in the simulation, and therefore, larger system can be considered at a reasonable time scale.

This report is organized as follows: in Chapter 2, background and literature reviews are provided, in Chapter 3, simulation studies of polyimide/OAPS and

polyimide/OHS mixed matrix materials are discussed; in Chapter 4, simulation studies of PDMS/OAPS and poly(imide siloxane)/OAPS are provided; in Chapter 5, a study of coarse-graining for OHS is discussed, and in Chapter 6, a summary of the work and future work are provided.

References

[1] Paul, D. R.; and Yampol'skii, Y. P. *Polymer Gas Separation Membranes: Introduction and Perspective*; CRC Press, 1994.
[2] Ievlev AL, Teplyakov VV. *Revue Roumaine De Chimie* **1990**, 35:831-842.
[3] Smolders CA, Reuvers AJ, Boom RM, Wienk IM. *J Membr Sci* **1992**, 73:259-275.
[4] Kreuer KD. *J Membr Sci* **2001**, 185:29-39.
[5] Caro J, Noack M, Kolsch P, Schafer R. *Microporous and Mesoporous Materials* 2000, 38: 3-24.
[6] C. M. Zimmerman, A. Singh, W. J. Koros, *J Membr. Sci.,* 137, 145-154 (1997).
[7] Pechar TW, Kim S, Vaughan B, Marand E, Baranauskas V, Riffle J, Jeong HK, Tsapatsis M. *J. Memb. Sci.* **2006**, 277:210-218.
[8] Husk GR, Cassidy PE, Gebert KL. *Macromolecules* **1988**, 21:1234-1238.
[9] Tishchenko G, Bleha M. *J Membr Sci* **2005**, 248:1-2.
[10] Strachota A, Tishchenko G, Bleha M. *J Inorg Organomet Pol* **2001**, 11:165-182.
[11] Iyer, P. and Coleman, M. R. *J. Appl. Pol. Sci.* **2008**, Vol. 108, 2691-2699.
[12] Leu, CM.; Chang, YT.; Wei, KH. *Chemistry of Materials* **2003**, 15, 3721-3727.
[13] Huang JC, He CB, Xiao Y, Mya KY, Dai J, Siow YP. *Polymer* **2003**, 44:4491-4499.
[14] Striolo, A.; McCabe, C.; Cummings, P. T. J. *Phys. Chem. B* **2005**, 109, 14300.
[15] Striolo A, McCabe C, Cummings PT. *J Chem Phys* **2006**, 125, 104904.
[16] Izvekov, S.; Parrinello, M.; Burnham, C. J.; Voth, G. A. *J. Chem. Phys.* **2004**, 120, 10896.
[17] Pranami G, Slipchenko L, Lamm MH, Gordon MS. *Coarse-grained intermolecular potentials derived from the effective fragment potential: Application to water, benzene, and carbon tetrachloride, chapter in Multi-Scale Quantum Models for Biocatalysis: Modern Techniques and Applications, in the Series, Challenges and Advances in Computational Chemistry and Physics*, Springer Verlag

CHAPTER 2 BACKGROUND AND LITERATURE REVIEWS

2.1 Mixed-Matrix Membranes

The limitation of polymeric membrane which is not able to withstand elevated temperature has brought the attention to many researchers to develop membranes with the incorporation of inorganic fillers in polymer matrix. This type of membrane is called mixed-matrix membrane (MMM). The purpose of making this membrane is to combine the advantages of the processability, permeability, and low cost of the polymers with the rigidity and high selectivity of the fillers. Figure 1 shows a schematic of mixed-matrix membrane that incorporates inorganic fillers within polymer matrix.

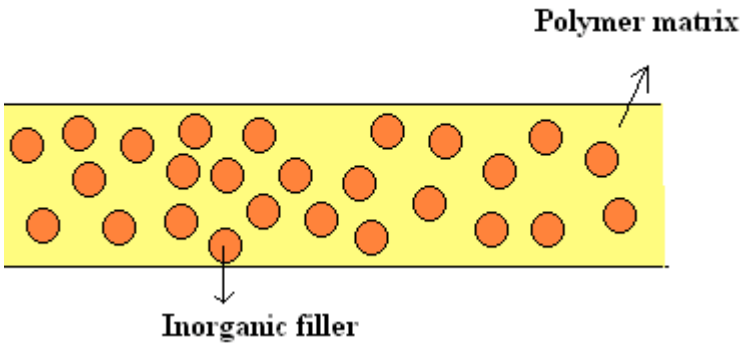

Figure 1: Mixed-Matrix Membrane

One important property to observe in a mixed matrix membrane is the glass transition temperature. A MMM with high glass transition temperature is desired especially for gas separation because an elevated temperature operating condition is usually required for that application. The incorporation of the inorganic fillers is expected to increase the glass transition temperature of the MMM. If there is a good contact between polymer matrix and the surface of the inorganic fillers, the glass transition temperature will usually increase. On the other hand, if there is a poor contact between those two materials, the glass transition temperature will decrease. The poor contact

between the polymer and the inorganic fillers may also lead to a macroscopic void, which results to a nonselective pathway of gas transport. Therefore, in order to design a robust membrane for gas separation applications, the proper selection of the polymer matrix and the proper selection of the inorganic filler are important.

The early works have focused on using rubbery polymer matrix in making MMMs [1], [2], [3], [4]. It has been reported that rubbery polymers performed a good contact with inorganic fillers such as, zeolites, which resulted a significant increase in selectivity for the membrane. This is true especially at high loading of the fillers [2], [3], [5]. On the other hand, due to the flexible nature of a rubbery polymer, it may have the lack in mechanical stability at high temperature [5].

Glassy polymers have also been of interest in designing the mixed matrix membranes. The glassy polymer may be able to withstand a high temperature. This is an advantage for the membranes, especially for gas separation applications. However, a poor compatibility between the glassy polymer and the inorganic filler may lead to the formation of voids between the two phases. These voids can reduce the separation performance of the membrane [6]. Some methods have been proposed to eliminate these gaps, such as: (i) by modifying the surface of the fillers with coupling agents to promote favorable interactions between polymer and the fillers [7], (ii) by adding plasticizer to promote the flexibility of polymers [6], [8], (iii) by forming hydrogen bonding between the two components [9], [10], or (iv) by forming the membrane at a temperature close to the glass transition temperature of the polymer to maintain its flexibility [8].

In addition, a block copolymer containing both flexible and rigid polymer segments has also been used in making the mixed matrix membranes [6]. Pechar *et al.* [6]

has designed a mixed matrix membrane using polydimethylsiloxane (PDMS)-polyimide block copolymer and zeolite fillers as the materials. The flexible segment, PDMS block will promote a good contact of the polymer to the fillers, on the other hand, the rigid segment, polyimide block will have higher selectivity compared to the PDMS segment. Their observations showed no evidence of the polymer being separated from the zeolites, which suggested a good dispersion of those two components. Their results have also shown an increase of the membrane's permeability for He, CO_2, O_2, N_2, and CH_4 gases with the use of 22 and 41 wt% of PDMS in the block copolymer.

As mentioned earlier, the proper choice of the inorganic fillers is another important thing to consider in creating a mixed matrix membrane. The most common inorganic fillers that have been used experimentally are carbon molecular sieves (CMSs) [11] and zeolite [6], [12]. Zeolites have been used as a filler in making mixed-matrix membrane with poly(vinyl acetate) (PVAc) [13], polyimide (a glassy polymer) [6], polyethersulfone [5], [14], poly(vinyl alcohol) (PVA) [15], polydimethylsiloxane (a rubbery polymer) [16], and polyetherimide [17]. CMSs have been incorporated into different polymers to form a mixed matrix membrane, for example, in polyimide [18], poly(ethylene glycol) [19], poly(vinylpyrrolidone) kollidone 15 or PVP K-15 [20], and poly(imide siloxane) [21].

It has been shown experimentally that the presence of inorganic fillers in the membrane materials can increase the selectivities of membranes. Suer *et al.* [14] has studied MMM of a glassy polymer, polyethersulfone (PES) and hydrophilic zeolites 13X and 4A. Their observation showed a significant enhancement in permeabilities and selectivities of the membrane at high loading of zeolite. Vu *et al.* [18] has incorporated

carbon molecular sieves within two different polymer matrices to form MMM for gas separations. Their results showed that the incorporation of the carbon molecular sieve enhanced the permeability and selectivity of the mixed matrix membrane. Recently, a lot of research have focused on the used of polyhedral oligomeric silsesquioxane (POSS) molecules as the inorganic filler. This filler has been used to modify mechanical and thermal properties of polymers.

2.2 Polyhedral Oligomeric Silsesquioxanes (POSS) and Its Applications

POSS $(RSiO_{1.5})_n$ where R is an organic functional group, has a unique cage-like structure. Due to the nanoscale dimension of POSS, it has been of particular interest in a lot of research areas. The possible POSS structures, such as $(RSiO_{1.5})_8$ (T_8-POSS), $(RSiO_{1.5})_{10}$ (T_{10}-POSS), $(RSiO_{1.5})_{12}$ (T_{12}-POSS) are shown in Figure 2. T_n denotes that there are *n* atoms found in the largest face of the cage. The most common studied POSS is the T_8-POSS.

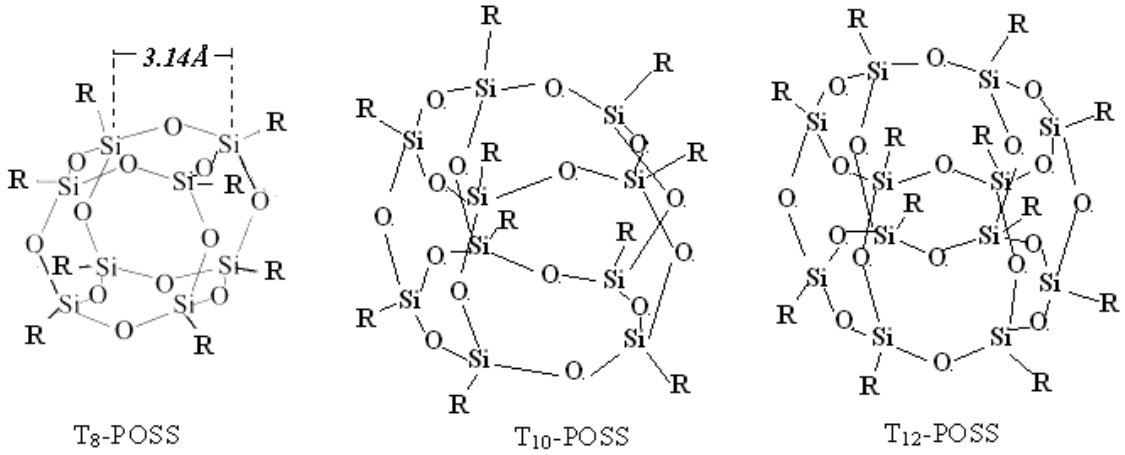

Figure 2: Structure of T_8-POSS, T_{10}-POSS, and T_{12}-POSS cages

Experimental works of POSS were first done with the focus of determining the variety of its crystal structures [22], [23], [24]. Barry *et al*. [25] determined the crystal structure of octamethyl silsesquioxane. Larsson [24] observed the crystal structures of

octa-(alkylsilsesquioxanes). Auf der Heyde *et al*. [26] has obtained the starting unit cell fractional coordinates for octahydrido silsesquioxanes, $H_8Si_8O_{12}$. They found out that the crystal arrangement is hexagonal with a unit cell contained three molecules.

The possibility to synthesize POSS with different functional groups results in many potential application areas for POSS-based materials, for example, as additives to paints and coatings [27], [28], [29] as well as in packaging materials and advanced plastics where POSS enhances temperature resistance [30], [31], [32], [33].

It has been pointed out in the literature that the functional groups present on POSS influence its important physical properties such as melting point and crystal structure [32], [34]. Thus, in order to determine these properties, many synthetic methods have been developed to explore how select organics groups modify the properties of POSS [35], [36]. Laine *et al*. [36] described methods of synthesizing POSS with liquid crystalline and polymerizable organic moieties. They synthesized octavinyldimethylsiloxy-functionalized POSS and octahydridodimethylsiloxy-functionalized POSS to produce material with well-defined microporosity and high surface area. The two different functional groups were able to produce material with different pore size distribution. Larsson [24] has determined different crystal structures of POSS with different alkyl functional groups. Ionescu *et al*. [32] has shown different crystal structure parameters obtained for octahydrido-functionalized and octamethyl-functionalized POSS.

POSS has also commonly been incorporated in polymers to form nanocomposite materials. There are different ways of incorporating POSS in polymers, such as by physically blending the POSS molecules with the polymer [34], by introducing them as

pendant groups on the polymer chain [37], [38], or by covalent binding within the polymer backbone [38], [39]. The incorporation of POSS molecules into a polymer results in improved material properties such as increased thermal stability, increased glass transition temperature, improved heat resistance, and reduction in flammability and heat evolution [27], [28], [33], [40], [41]. Lee *et al*. [42], Leu *et al*. [43] and Chen *et al*.[44] have incorporated POSS into a polyimide polymer backbone for low dielectric film applications. POSS has also been incorporated as pendant groups in polynorbornene [45], methacrylate [46], poly 4-methylstyrene [47], polystyrene [48] and polyoxazolines [49]. In addition, some previous works have blended POSS with poly(methylvinylsiloxane) [50], poly(dimethylsiloxane) [34], and polystyrene [51].

Iyer and Coleman [52] studied blends of polyimide (PI) with octaphenyl silsesquioxane (OPS) and with octaaminophenyl silsesquioxane (OAPS). Their results for PI-OPS composites showed a visible phase separation at 5 wt % OPS loading. This has caused a lower glass transition temperature of the PI-OPS composites material compared to the T_g of the pure PI. They have also shown that functionalizing OPS with amine groups enhanced thermal and mechanical stability of the composites. This was shown by higher glass transition temperatures found for the PI-OAPS composites compared to the pure PI. The higher glass transition temperature suggested favorable interactions between PI and OAPS. In their experiments, a transparent composite with well-dispersed OAPS was produced. They reported that good thermal stability of the composite was obtained with up to 20 wt% OAPS loading.

2.3 Simulation Studies of POSS

Although the number of experimental studies about the incorporation of POSS in polymeric materials has grown, there are still a lot more to understand concerning the effect of POSS on the thermal properties of the materials [38], [53] and whether POSS molecules are uniformly dispersed within the polymer or form aggregates [34], [54], [55]. All these behaviors may affect the thermal properties of the materials. Particularly, the orientation of the POSS molecules and also the interactions between POSS to the polymer are the main problems of the study. In the last decade, molecular simulations have contributed to our knowledge about the fundamental interactions between polymer and POSS species. Not only that simulation studies [37], [56], [57] have shown a good agreement of the thermal properties of POSS-polymer systems to the experimental results, molecular simulation can also provide a molecular insight of the properties of POSS in polymer matrix.

Bharadwaj *et al.* [37] studied the effects of POSS moieties onto polymeric chains as pendant groups using atomistic molecular dynamics simulations. They found out that the incorporation of POSS with cyclopentyl rings and POSS with cyclohexyl rings on polynorbornene chains lead to an increase in the glass transition temperature of the material. Their simulation results on glass transition temperature agreed favorably to the experimental results. They have also presented that different functional groups of POSS affected on how the polymer chain packed around the POSS molecules. Striolo *et al.* [34] used molecular dynamics algorithms to study the thermodynamic and transport properties of octahydrido and octamethyl silsesquioxanes blended in poly(dimethylsiloxane)

(PDMS). Their results showed that POSS tend to attract to each other when dissolved in PDMS.

Capaldi *et al*. [58] simulated blends of cyclopenthyl-substituted POSS (CpPOSS) on a polyethylene (PE) matrix. They studied three different systems which contained 5, 15, and 25 wt% of CpPOSS. Their observation showed a strong tendency of POSS particles to crystallize at room temperature. Patel *et al*. [56] conducted molecular dynamics simulations to study the effect of the incorporation of T_8, T_{10} and T_{12}-POSS monomers with various organic substituents onto the properties of polystyrene and poly(methyl methacrylate) (PMMA). In their study, POSS monomers were chemically bonded on the polymer matrix to form copolymer. Their results showed an increase in glass transition temperature with the incorporation of POSS in polystyrene system, and a decrease in the glass transition temperature with the incorporation of POSS in PMMA system.

Bizet *et al.* [57] has performed an atomistic molecular dynamics simulation to investigate the effect of the incorporation of (Isobutyl)$_7$Si$_8$O$_{12}$(propyl methacrylate) (*i*BuPOSS) and (cyclohexyl)$_7$Si$_8$O$_{12}$(propyl methacrylate) (CyPOSS) as pendant groups on the polymethyl methacrylate (PMMA) backbone. Their results showed a good agreement between simulated X-ray scattering intensities with the experimental results. Their simulation observations have also shown an increase of the glass transition temperature with the incorporation of CyPOSS and a decrease of the glass transition temperature with the incorporation of *i*BuPOSS, which were also in agreement with the experimental data.

2.4 Coarse-Grained Method

Although the atomistic simulation is able to provide a good understanding of the effect of the POSS incorporation into a polymer matrix to the thermal properties, it has a limitation to the size of a system being observed. In practical applications, it usually requires a larger system size, which means a larger simulated time scales will be needed. In order to overcome this situation, a further simplification of the atomistic model is necessary. Coarse-grained (CG) approaches have been known with such objective. To apply the coarse-grained method in an atomistic system, first, atoms are grouped together to represent a coarse-grained site. This scheme can be seen in Figure 3. The coarse-grained site is usually the center of mass or geometric center of the atom groups. Then, the effective interaction potentials between the coarse-grained sites are determined. These potentials are then used in the CG simulation to obtain properties, which are comparable to the atomistic simulation.

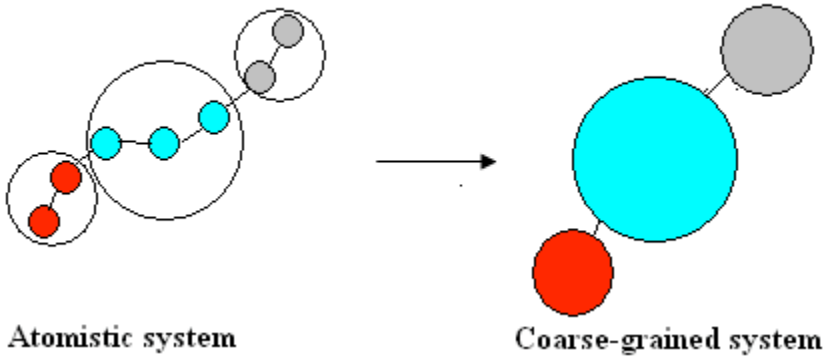

Figure 3: Coarse-graining scheme

Some approaches to obtain the potentials in coarse-graining include: optimizing the potential parameters by fitting it to the desired property [59], [60], [61]; by structure matching [62], or by force matching (FM) [63], [64]. Shelley *et al*. [59] developed a

coarse grained model for phospholipids by fitting the potential parameters to mimic the structural properties similar to the atomistic simulations or experiment. Three water molecules were grouped to represent one spherical CG site. The interactions followed the Lennard-Jones 6-4 potential. $(CH_2)_3$, $(CH_2)_2$-CH_3, choline, phosphate, glycerol backbone, and ester groups were represented as one CG site. The parameters for the harmonic bond potential and the angle potential were fitted to reproduce the average and deviation of the corresponding length obtained from atomistic simulations. The parameters for the nonbonded interactions were obtained such that the radial distribution function obtained from the CG model matched the radial distribution function obtained from the atomistic model. Their CG model was fast and able to semi-quantitatively reproduce the density profile of the bilayer. However, this model may be only limited to the interaction potential that involves the influence of solvent. It is also tedious since it involves different method for different coarse-grained sites.

Harmandaris *et al*. [61] derived a coarse-grained model for polystyrene in which one monomer was represented by two CG sites. The bonded interaction potentials which include bond, angle, and dihedral were determined by sampling distribution functions in united atom simulations of polystyrene dimmers. The nonbonded interaction potential was modeled using an offset and shifted Lennard-Jones 12-6 potential. Their results showed that the radius of gyration, end-to-end distance, and the distribution function of bonds, bending and dihedral angles of polystyrene chains obtained from their coarse-grained model were in excellent agreement with the one obtained from the atomistic MD simulations.

This work will focus on the force-matching method. The force-matching method can determine a pairwise force field from a given trajectory and force data from *ab initio* simulation or atomistic molecular dynamics simulation. This method was first introduced by Ercolessi and Adams [63]. They determined a method for least-squares fitting of the potential to the force data calculated from *ab initio* calculation [64]. Their force-matching method was mainly applied to elemental systems, such as metals.

Izvekov *et al*. [64] then developed a new force-matching method that can only parametrize the classical force field if it is linearly dependent on the fitting parameters. This can usually be achieved through spline interpolations. The Voth group has successfully employed this method to obtain the CG model of dimyristoylphosphatidylcholine (DPMS) lipid bilayer [65]. Their CG model was able to reproduce the structural properties of a lipid bilayer from the atomistic simulation. It was also stated that their approach was computationally not expensive. The force-matching method has also been successfully employed to obtain the CG model of condensed-phase systems [64], [66]; ionic liquids [67], [68], and also C_{60} and carbonaceous nanoparticles [69].

References

[1] Te Hennepe HJC, Bargeman D, Mulder MHV, Smolders CA. *J Membr Sci* **1987**, 35:39-55.
[2] Jia M, Peinemann KV, Behling RD. *J Membr Sci* **1991**, 57:289-292.
[3] Duval JM, Folkers B, Mulder MHV, Desgrandchamps G, Smolders CA. *J Membr Sci* **1993**, 80:189-198.
[4] Koros WJ, Mahajan R. *Ind Eng Chem Res* **2000**, 39:2692-2696.
[5] Li Y, Chung TS, Cao C, Kulprathipanja S. *J Membr Sci* **2005**, 260:45-55.
[6] Pechar TW, Kim S, Vaughan B, Marand E, Baranauskas V, Riffle J, Jeong HK, Tsapatsis M. *J. Memb. Sci.* **2006**, 277:210-218.

[7]Duval JM, Kemperman AJB, Folkers B, Mulder MHV, Desgrandchamps G, Smolders CA. *J Appl Polym Sci* **1994**, 54:409.
[8] Mahajan R, Burns R, Schaeffer M, Koros WJ. *J Appl Pol Sci* **2002**, 86:881-890.
[9] Yong HH, Park HC, Kang YS, Won J, Kim WN. *J Membr Sci* **2001**, 188, p 151.
[10] Mahajan R, Koros WJ. *Polym Eng Sci* **2002**, 42:1432-1441.
[11] Jiang, LY, Chung TS, Rajagopalan R. Carbon 2007, 45: 166-172.
[12] Tin PS, Chung TS, Jiang LY, Kulprathipanja S. *Carbon* **2005**, 43:2025.
[13] Mahajan R, Koros WJ. Ind Eng Chem Res **2000**, 39:2692-2696.
[14] Suer MG, Bac N, Yilmaz L. *J Memb. Sci* **1994**, 91:77-86.
[15] Guan HM, Chung TS, Huang Z, Chng ML, Kulprathipanja S. *J Membr Sci* **2006**, 268:113-122.
[16] Tantekin-Ersolmaz SB, Atalay-Orala C, Tather M, Erdem-Senatalar A, Schoeman B, Sterte J. *J Membr Sci* **2000**, 175:285-288.
[17] Husain S, Koros WJ. *J Membr Sci* **2007**, 288:195-207.
[18] Vu DQ, Koros WJ, Miller SJ. *J Memb. Sci* **2003**, 211:311-334.
[19] Zhang XY, Hu HQ, Zhu YD, Zhu SW. *J Membr Sci* **2007**, 289:86-91.
[20] Rafizah WAW, Ismail AF. *J Membr Sci* **2008**, 307:53-61.
[21] Park HB, Jung CH, Kim YK, Nam SY, Lee SY, Lee YM. *J Membr Sci* **2004**, 235:87-98.
[22] Larsson, K. Ark. Kemi 1960, 16, 215.
[23] Larsson, K. Ark. Kemi 1960, 16, 203.
[24] Larsson, K. Ark. Kemi 1960, 16, 209.
[25] Barry AJ, Daudt WH, Domincone JJ, Gilkey JW. *J Am Chem Soc* 1955, 77:4248.
[26] Auf der Heyde, T. P. E.; Burgi, H. B.; Burgy, H.; Tornroos, K. W. *Chimia* **1991**, 45, 38.
[27] Dodiuk, H.; Rios, P. F.; Dotan, A.; Keniq, S. *Pol. Adv. Tech.* **2007**, 18, 746-750.
[28] Oaten, M.; Choudhury, N. R. *Macromolecules* **2005**, 38, 6392-6401.
[29] Devaux, E.; Rochery, M.; Bourbiqot, S. *Fire and Materials* **2002**, 26, 149-154.
[30] Laine, R. M. *J. Mater. Chem.* **2005**, 15, 3725.
[31] Peng, Y.; McCabe, C. *Mol. Phys.* **2007**, 105, 261.
[32] Ionescu, T. C.; Qi, F.; McCabe, C.; Striolo, A.; Kieffer, J.; Cummings, P. T. *J. Phys. Chem. B* **2006**, 110, 2502.
[33] Pielichowski, K.; Njuguna, J.; Janowski, B.; Pielichowski, J. *Adv. Polym. Sci.* **2006**, 201, 225-296.
[34] Striolo, A.; McCabe, C.; Cummings, P. T. J. *Phys. Chem. B* **2005**, 109, 14300.
[35] Voss, E. J.; Sabat, M.; Shriver, D. F. *Inorg. Chem.* **1991**, 30, 2707.
[36] Laine, R. M.; Zhang, C.; Sellinger, A.; Viculis, L. *Appl. Organometal. Chem.* **1998**, 12, 715.
[37] Bharadwaj, R. K.; Berry, R. J.; Farmer, B. L. *Polymer* **2000**, 41, 7209.
[38] Lichtenhan, J. D. *Comm. Inorg. Chem.* **1995**, 17, 115-130.
[39] Mark, J. E. *Macromol. Symp.* **2003**, 201, 77-83.
[40] Li, GZ.; Wang, LC.; Ni, HL.; Pittman Jr., C. U. *J. Inorg. Organomet. Pol.* **2001**, 11, 123-154.
[41] Schwab, J. J.; Lichtenhan, J. D. *Appl. Organometal. Chem.* **1998**, 12, 707-713.

[42] Lee, YJ; Huang, JM; Kuo, SW; Lu, JS; Chang, FC *Polymer* **2005**, 46, 173-181.
[43] Leu, CM.; Chang, YT.; Wei, KH. *Chemistry of Materials* **2003**, 15, 3721-3727.
[44] Chen, YW.; Kang, ET. *Materials Letters* **2004**, 58, 3716-3719.
[45] Mather, P. T.; Jeon, H. G.; Romo-Uribe, A. *Macromolecules* **1999**, 32, 1194-1203.
[46] Lichtenhan, J. D.; Otonari, Y. A.; Carr, M. J. *Macromolecules* **1995**, 28, 8435-8437.
[47] Romo-Uribe, A.; Mather, P. T.; Haddad, T. S.; Lichtenhan, J. D. *J. Poly. Sci.B Polym. Phys.* **1998**, 36, 1857-1872.
[48] Haddad, T. S.; Lichtenhan, J. D. *Macromolecules* **1996**, 29, 7302.
[49] Kim, K. M.; Keum, D. K.; Chujo, Y. *Macromolecules* **2003**, 36, 867-875.
[50] Liu, L.; Tian, M.; Zhang, W.; Zhang, LQ; Mark, J. E. *Polymer* **2007**, 48, 3201-3212.
[51] Liu, L.; Hu, Y.; Song, L.; Nazare, S.; He, SQ.; Hull, R. *J. Mat. Sci.* **2007**, 42, 4325-4333.
[52] Iyer, P. and Coleman, M. R. *J. Appl. Pol. Sci.* **2008**, Vol. 108, 2691-2699.
[53] Xu, H.; Kuo, JW.; Lee, JS.; Chang, FC. *Macromolecules* **2002**, 35, 8788-8793.
[54] Fu, B. X.; Hsiao, B. S.; Pagoda, S.; Stephens, P.; White, H.; Rafailovich, M.; Sokolov, J.; Mather, P. T.; Jeon, H. G.; Phillips, S.; Lichtenhan, J.; Schwab, J. *Polymer* **2001**, 42, 599.
[55] Zheng, L.; Farris, R. J.; Coughlin, E. B. *Macromolecules* **2001**, 34, 8034-8039.
[56] Patel, R. R.; Mohanraj, R.; Pittman JR., C. U. *J. Polym. Sci.: Part B: Polym. Phys.* **2006**, Vol. 44, 234-248.
[57] Bizet S, Galy J, Gerard JF. *Polymer* **2006**, 47:8219-8227.
[58] Capaldi, F. M.; Rutledge, G. C.; Boyce, M. C. *Macromolecules* **2005**, 38, 6700-6709.
[59] Shelley JC, Shelley MY, Reeder RC, Bandyopadhyay S, Klein ML. *J Phys Chem B* **2001**, 105:4464-4470.
[60] Shelley JC, Shelley MY, Reeder RC, Bandyopadhyay S, Moore PB, Klein ML. *J Phys Chem B* **2001**, 105:9785-9792.
[61] Harmandaris VA, Adhikari NP, van der Vegt NFA, Kremer K. *Macromolecules* **2006,** 39, (19), 6708-6719.
[62] McGreevy RL, Pusztai L. *Molecular Simulation* **1988,** 1, (6), 359 - 367.
[63] Ercolessi F, Adams JB. *Europhys Lett* **1994**, 26:583-588.
[64] Izvekov, S.; Parrinello, M.; Burnham, C. J.; Voth, G. A. *J. Chem. Phys.* **2004**, 120, 10896.
[65] Izvekov, S.; Voth, G. A. *J. Phys. Chem. B* **2005**, 109, 2469.
[66] Izvekov S, Voth GA. *J Phys Chem B* **2005,** 109, (14), 6573-6586.
[67] Wang YT, Izvekov S, Yan TY, Voth GA. *J Phys Chem B* **2006,** 110, (8), 3564-3575.
[68] Wang YT, Izvekov S, Yan TY, Voth GA. *J Phys Chem B* **2006,** 110, (37), 18601-18608.
[69] Izvekov S, Violi A, Voth GA. *J Phys Chem* **2005**, 109 (36), 17019-17024.

CHAPTER 3 MOLECULAR DYNAMICS SIMULATION OF MIXED MATRIX NANOCOMPOSITES CONTAINING POLYIMIDE AND POLYHEDRAL OLIGOMERIC SILSESQUIOXANE (POSS)

(A paper published in *Polymer* **2009**, Vol. 50, 1324-1332)

Yin Yani and Monica H. Lamm

Abstract

Mixed matrix blends containing polyimide (PI) and polyhedral oligomeric silsesquioxanes (POSS) are studied with atomistic molecular dynamics simulation. To examine the effect of functional group, two types of POSS are considered, either octahydrido silsesquioxane (OHS) or octaaminophenyl silsesquioxane (OAPS). The glass transition temperature of the model PI-OAPS blends increases with the incorporation of OAPS, an observation consistent with recent experiments on these systems. A decrease in glass transition temperature is shown for the model PI-OHS blends. Radial distribution functions for both blends are presented to show how packing between the inorganic (POSS) and organic (PI) species in the mixed matrix varies as a function of POSS loading and POSS functionalization. In addition, we report the mobility of the PI chains and POSS molecules in the material by calculating the mean square displacement. These results provide molecular insight about thermal property enhancements afforded by POSS-based additives.

Keywords: Polyhedral oligomeric silsesquioxane; Polyimide; Molecular dynamics simulations

3.1 Introduction

Membranes have been widely used in gas separation applications, such as for hydrogen purification, hydrogen recovery in oil refinery processes, air purification, and natural gas processing. Membranes were first introduced for gas separation by J. K. Mitchell of Philadelphia in 1831 [1]. The most commonly used membranes in industry are made from polymers. Polymeric membranes are cost effective, easy to process, and have good gas transport properties. The main drawback for this type of membrane is the inability to withstand elevated temperatures. At high temperatures, the mobility of individual polymer chains increases which results in poor selectivity for the membranes. Therefore, polymer membranes cannot be used to produce gases of high purity. Other types of membranes that have been used for gas separation are inorganic membranes. This type of membrane has good permeability and comparable selectivities for gases at elevated temperature. However, inorganic membranes are difficult to process and less cost effective compared to polymeric membranes. Therefore, attention has focused on the development of another type of membrane, mixed-matrix nanocomposites [2], which incorporate an inorganic molecular sieve within the polymeric matrix.

Mixed-matrix nanocomposites are a high performance material that combine the advantages of inorganic fillers and polymeric materials. Polyhedral oligomeric silsesquioxanes (POSS) are one of the inorganic fillers that have been used for this purpose. POSS has the chemical composition of $(RSiO_{1.5})_n$ with R as an organic functional group. The possibility to synthesize POSS with different functional groups results in many potential application areas for POSS-based materials, for example, as

additives to paints and coatings, [3], [4], [5] as well as in packaging materials and advanced plastics where POSS enhances temperature resistance [6], [7], [8], [9].

The functional groups on POSS may affect the physical properties such as melting point and crystal structure [8], [10]. Thus, in order to determine these properties, many synthetic methods have been developed to explore how select organics groups modify the properties of POSS [11], [12]. Laine *et al.* [12] described methods of synthesizing POSS with liquid crystalline and polymerizable organic moieties. They synthesized octavinyldimethylsiloxy silsesquioxane and octahydridodimethylsiloxy silsesquioxane to produce material with well-defined microporosity and high surface area. The two different functional groups were able to produce materials with different pore size distribution.

The impact of functional group on POSS materials has also been studied computationally. Ionescu *et al.* [8] used molecular dynamics simulation to show that octahydrido silsesquioxane (OHS, R = H) yields a different crystal structure than the crystal structure of octamethyl silsesquioxane. Striolo *et al.* reported the molecular simulation results for the radial distribution function and the effective pair potentials of mean force between OHS and between octamethyl silsesquioxanes in normal hexadecane [13], poly(dimethylsiloxane) [13], and normal hexane [14] solvents; and between POSS-alkane telechelic hybrid monomers in normal hexane [15] solvent. Their results have shown that replacing the hydrogen atoms in OHS with methyl groups alters the effective POSS-POSS interactions.

POSS can be incorporated in polymers to form nanocomposite materials in different ways, such as by physically blending the POSS molecules with the polymer

[10], by introducing them as pendant groups on the polymer chain [16], [17], or by covalent binding within the polymer backbone [17], [18]. The incorporation of POSS molecules into a polymer results in improved material properties such as increased thermal stability, increased glass transition temperature, improved heat resistance, and reduction in flammability and heat evolution [3], [4], [9], [19], [20]. Lee *et al.* [21], Leu *et al*. [22] and Chen *et al.* [23] have incorporated POSS into a polyimide polymer backbone for low dielectric film applications. POSS has also been incorporated as pendant groups in polynorbornene [24], methacrylate [25], poly 4-methylstyrene [26], polystyrene [27] and polyoxazolines [28]. In addition, some previous works have blended POSS with poly(methylvinylsiloxane) [29], poly(dimethylsiloxane) [10], and polystyrene [30].

Iyer and Coleman [31] studied blends of polyimide (PI) with octaphenyl silsesquioxane (OPS, R = C_6H_5) and with octaaminophenyl silsesquioxane (OAPS, R = $C_6H_4(NH_2)$). Their results for PI-OPS composites showed a visible phase separation at 5 wt % OPS loading. They have also shown that functionalizing OPS with amine groups enhanced thermal and mechanical stability of the composites. This was shown by higher glass transition temperatures found for the PI-OAPS composites compared to the pure PI. The higher glass transition temperature suggested favorable interactions between PI and OAPS. In their experiments, a transparent composite with well-dispersed OAPS was produced. They reported that good thermal stability of the composite was obtained with up to 20 wt% OAPS loading.

Although the number of experimental studies about the incorporation of POSS in polymeric materials has grown, there is still a lot more to understand concerning the

effect of POSS on the thermal properties of the materials [17], [32] and whether POSS molecules are uniformly dispersed within the polymer or form aggregates [10], [33], [34]. In the last decade, molecular simulations have contributed to our knowledge about the fundamental interactions between polymer and POSS species. Bharadwaj *et al.* [16] studied the effects of POSS moieties onto polymeric chains as pendant groups using atomistic molecular dynamics simulations. They found out that the incorporation of POSS with cyclopentyl rings and POSS with cyclohexyl rings on polynorbornene chains lead to an increase in the glass transition temperature of the material. They have also shown that different functional groups on POSS affect how the polymer chain packed around the POSS molecules.

Striolo *et al.* [10] used molecular dynamics simulations to study the thermodynamic and transport properties of OHS and octamethyl ($R = CH_3$) silsesquioxanes dissolved in poly(dimethylsiloxane) (PDMS). Their results showed that POSS tend to attract to each other when dissolved in PDMS. Capaldi *et al.* [35] simulated blends of cyclopentyl-substituted POSS (CpPOSS) in a polyethylene (PE) matrix. They studied three different systems which contained 5, 15, and 25 wt% of CpPOSS. Their observation suggested a strong tendency of POSS particles to crystallize at room temperature. Patel *et al.* [36] conducted molecular dynamics simulations to study the effect of the incorporation of T_8, T_{10} and T_{12}-POSS monomers with various organic substituents onto the properties of polystyrene and poly(methyl methacrylate) (PMMA). In their study, POSS monomers were covalently bonded to the polymer matrix to form copolymer. Their results showed an increase in glass transition temperature with the

incorporation of POSS in the polystyrene system, and a decrease in the glass transition temperature with the incorporation of POSS in the PMMA system.

In addition to the atomistic simulations discussed above, there is an alternative approach, called a coarse-grained (CG) model that has been used for POSS/polymer systems. A CG model eliminates the unimportant degrees of freedom in the simulation by treating a collection of atoms as one coarse-grained site, and therefore, larger systems can be considered at longer time scales. Chan *et al.* [37] has developed a CG model using a structural-based scheme to simulate self-assembly for nonyl-tethered POSS molecules dissolved in hexane solvent. Their results showed a small aggregate of POSS molecules, which is similar to the one obtained with atomistic simulations. They also reported that their CG model reduced computational time by about two orders of magnitude compared to simulations with the equivalent atomistic model.

Despite the above efforts, there are still a lot of unanswered questions about the formation and properties of POSS/polymer composites that need to be addressed, such as whether a different type of POSS will yield different thermodynamic properties for a POSS/polymer system, or whether a different loading of POSS will induce different packing of POSS and polymer in the material. In this work, we analyze the effect that incorporation of different POSS within a polyimide matrix has on the thermal properties of the nanocomposite. We provide a detailed molecular dynamics simulation study of POSS molecules blended with a polyimide (PI) polymer chain. Two types of POSS molecules will be considered: (i) POSS with hydrogen functional groups (OHS) and (ii) POSS with aminophenyl functional groups (OAPS). The paper is organized as follows: in Section 2, a detailed explanation of the force fields used in this work is provided and the

molecular dynamics simulation method is explained; in Section 3, the simulation results are discussed and compared to the available experimental results; and in Section 4, a summary of the findings is provided.

3.2 Molecular Models and Simulation Methods

3.2.1 Molecular models

The systems studied consist of 2,2-bis(3,4-dicarboxyphenyl)-hexafluoropropane dianhydride (6FDA)/4,4'-diaminediphenylmethane (MDA) polyimide (PI) [31], octahydrido silsesquioxane (OHS)/PI blends and octaaminophenyl silsesquioxane (OAPS)/PI blends. The chemical structure for the PI repeat unit is shown in Figure 1. The molecular weight of the PI was 18196.4 g/mol, corresponding to a n = 30 monomer chain. The chemical structures for the two POSS species (OHS and OAPS) are shown in Figure 2. The POSS cage has an edge length (Si to Si) of 3.14 Å. The cube's edge length (H to H) for OHS is about 4.8 Å, and the cube's edge length (N to N) for OAPS is about 10 Å.

The TRIPOS 5.2 force field [38] was used to model the atomic interactions in PI. This force field has been used to model polyimides and other polymers that have a large number of aromatic rings [39], [40]. Physical properties that have been validated with the TRIPOS force field include cohesive energy, Hildebrand solubility parameters [39], and glass transition temperatures [40]. This force field consists of harmonic bond stretching (E_b), angle bending (E_θ), out-of-plane bending (E_χ), and torsion (E_ϕ) terms, which are shown in equation (1), (2), (3), and (4), respectively.

$$E_b = k_{ij}\left(d_{ij} - d_{ij}^{o}\right)^2 \tag{1}$$

$$E_\theta = k_{jkj}(\theta - \theta_o)^2 \tag{2}$$

$$E_{\chi} = kd^2 \tag{3}$$

$$E_{\phi} = k_{ijkl}\left(1 + s/|s| * \cos\left(|s|B_{ijkl}\right)\right) \tag{4}$$

where d_{ij} is the actual bond length, d_{ij}^{0} is the equilibrium bond length, θ is the actual bond angle, θ_0 is the equilibrium bond angle, d is the distance from the atom to the plane defined by its three attached atoms, B is the torsion angle, k, k_{ij}, k_{jkj}, k_{ijkl} and s are the constants. The nonbonded interactions include the van der Waals and the electrostatic potentials. The 6-12 Lennard Jones potential was used to model the van der Waals interaction.

$$u_{ij}(r) = 4\varepsilon_{ij}\left[\left(\frac{\sigma_{ij}}{r_{ij}}\right)^{12} - \left(\frac{\sigma_{ij}}{r_{ij}}\right)^{6}\right] \tag{5}$$

where ε_{ij} is the Lennard-Jones well-depth, σ_{ij} is the Lennard-Jones diameter, and r_{ij} is the distance between atom i and j. The electrostatic potential is expressed by

$$E_{coul} = \sum_{i,j} \frac{q_i q_j}{\varepsilon r_{ij}} \tag{6}$$

where q_i is the partial charge on atom i, and ε is the dielectric constant. The parameters and constants for the TRIPOS force field used for this work are given in Table 1. The partial charges were obtained by first doing *ab initio* calculations in GAMESS [41] (General Atomic and Molecular Electronic Structure System) with the [6-31G(d)] [42] basis set to get the ESP (electrostatic potential) charges. As shown in Figure 1b, we took one PI monomer and added part B to C1, and added part A to N23, and did the ab-initio calculations for [A-Monomer-B]. The R.E.D. (RESP ESP charge Derive) program [43] was then used to obtain the partial charges for the monomer fragment of the PI chain. These partial charges are listed in Table 2.

Table 1: Parameters Used in TRIPOS [38] Force Field for PI

E_b	d_{ij}^o (Å)	k_{ij}(kcal/mol- Å^2)
[a]C_{ar}-C_{ar}	1.395	1400.0
C_{ar}-H	1.084	692.0
C-F	1.360	600.0
C-O	1.220	1555.2
C_{ar}-N	1.346	1305.94
C-C	1.540	633.6
C-C_{ar}	1.525	640.0
C-H	1.100	662.4
N-H	1.080	692.0
N-N	1.418	1300.0
E_θ	θ_o (deg)	k_{ikj}(kcal/mol-rad^2)
C_{ar}-C_{ar}-C_{ar}	120.0	78.79
C-C-H	109.5	52.52
F-C-F	109.5	131.31
C-C-C_{ar}	109.5	78.79
C_{ar}-C-C_{ar}	109.5	59.09
C-C_{ar}-C_{ar}	120.0	78.79
H-C-H	109.5	78.79
C_{ar}-N-C_{ar}	120.0	131.31
C_{ar}-C_{ar}-N	120.0	78.79
N-C-O	120.0	85.35
C-N-H	119.0	52.52
C-N-N	118.0	131.31
E_χ	k (kcal/mol-Å^2)	
C_{ar}	480	
C	480	
N	120	
E_ϕ	k_{iklj} (kcal/mol)	s
C_{ar}-C-C-F	0.2	3
H-C_{ar}-C_{ar}-N	2.0	-2
H- N_{ar}-C_{ar}-O	1.6	-2
C_{ar}-C-C_{ar}-C_{ar}	0.12	-3
O-C-N-C	1.6	-2
E_{vdw}	σ_{ij} (Å)	ε_{ij}(kcal/mol- Å^2)
C_{ar}-C_{ar}	3.03	0.107
H-H	2.673	0.042
N-N	2.762	0.095
O-O	2.71	0.116
F-F	2.62	0.109

[a] aromatic carbon

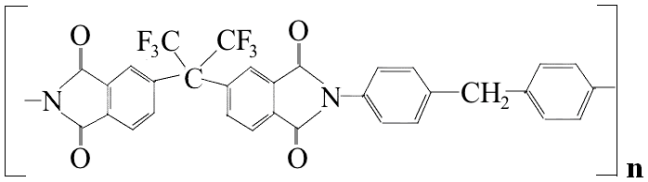

(a)

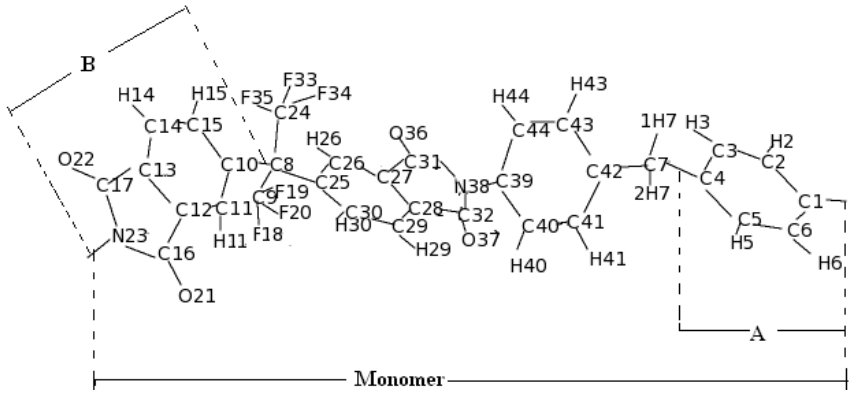

(b)

Figure 1: (a) Repeat unit of the 6FDA-MDA polyimide polymer chain (b) Schematic to define the atom labels used with partial charges in Table 2.

Table 2: Partial Charges for atoms in the PI monomer

Label	*q*	Label	*q*	Label	*q*	Label	*q*
C1	0.0774	C10	-0.0203	O22	-0.4822	F34	-0.1186
C2	-0.1910	C11	-0.0398	N23	-0.0715	F35	-0.1186
C3	-0.1295	C12	-0.0691	C24	0.3552	O36	-0.4777
C4	0.0451	C13	-0.0469	C25	-0.0092	O37	-0.4775
C5	-0.1295	C14	-0.1126	C26	-0.0468	N38	-0.0669
C6	-0.1910	C15	-0.1260	C27	-0.0604	C39	0.0718
H2	0.1627	C16	0.4581	C28	-0.0774	C40	-0.1958
H3	0.1304	C17	0.4864	C29	-0.1214	C41	-0.1260
H5	0.1304	H11	0.1362	C30	-0.1022	C42	0.0379
H6	0.1627	H14	0.1614	C31	0.4582	C43	-0.1260
C7	-0.0774	H15	0.1609	C32	0.5036	C44	-0.1958
1H7	0.0580	F18	-0.1186	H26	0.1409	H40	0.1640
2H7	0.0580	F19	-0.1186	H29	0.1647	H41	0.1350
C8	-0.1129	F20	-0.1186	H30	0.1525	H43	0.1350
C9	0.3552	O21	-0.4712	F33	-0.1186	H44	0.1640

The Hybrid-COMPASS (HC) force field [8], [44] was used to model the atomic interactions in OHS and OAPS. This force field includes bond stretching (E_b), angle bending (E_θ), and torsion (E_ϕ) terms which are described by equation (7), (8), and (9), respectively.

$$E_b = k_2(b-b_o)^2 + k_3(b-b_o)^3 + k_4(b-b_o)^4 \tag{7}$$

$$E_\theta = H_2(\theta-\theta_o)^2 + H_3(\theta-\theta_o)^3 + H_4(\theta-\theta_o)^4 \tag{8}$$

$$E_\phi = V_1(1-\cos(\phi)) + V_2(1-\cos(2\phi)) + V_3(1-\cos(3\phi)) \tag{9}$$

where b_o is the equilibrium bond length, θ_o is the equilibrium bond angle, b is the actual bond length, θ is the actual angle, ϕ is the actual value of the dihedral angle, k_2, k_3, k_4, H_2, H_3, H_4, V_1, V_2, and V_3 are constants. The Lennard Jones (LJ) 9-6 function (E_{vdw}) was used to model the van der Waals interactions,

$$U_{vdw} = \varepsilon_{ij}\left\{2\left[\frac{r_{ij}}{r}\right]^9 - 3\left[\frac{r_{ij}}{r}\right]^6\right\} \tag{10}$$

where ε_{ij} is the LJ well-depth potential, r_{ij} is the LJ distance between atoms, r is the actual distance of the atom pair.

$$r_{ij} = \left(\frac{r_i^6 + r_j^6}{2}\right)^{1/6} \tag{11}$$

$$\varepsilon_{ij} = \left(\frac{2r_i^3 r_j^3 \sqrt{\varepsilon_i \varepsilon_j}}{r_i^6 + r_j^6}\right) \tag{12}$$

where, r_i, r_j, ε_i, and ε_j represent the like atom interaction parameters for atom i and j, respectively. Table 3 shows the Hybrid-COMPASS force field parameters used for this work. The nonbonded interaction terms include the Coulombic function (E_{coul}) for

electrostatic interactions, which is shown in Eq. (6). In the HC force field, the partial charge q_i is given by

$$q_i = \sum_j \delta_{ij} \tag{13}$$

where δ_{ij} is the bond increment for an atom j that is valence bonded to atom i. However, in this work, the partial charges shown in Table 4 were obtained from *ab initio* calculations done in GAMESS [41] with [6-31G(d)] [42] basis set. Recently, Li *et al.* [45] reported partial charges for OHS and these are shown in Table 4 for comparison.

Table 3: Parameters Used in HC Force Field [8], [44] for OHS and OAPS

E_b	b_o (Å)	k_2 (kcal/mol- Å^2)	k_3 (kcal/mol- Å^3)	k_4 (kcal/mol- Å^4)
Si-C	1.899	189.65	-279.42	307.51
Si-O	1.640	359.123	-517.342	673.707
Si-H	1.478	202.78	-305.36	280.27
C_{ar}-C_{ar}	1.417	470.836	-627.618	1327.635
C-H	1.0982	372.825	-803.453	894.317
C-N	1.400	350.0	0.0	0.0
N-H	1.031	540.112	-1500.295	2431.008
E_θ	θ_o (deg)	H_2 (kcal/mol- rad^2)	H_3 (kcal/mol- rad^3)	H_4 (kcal/mol- rad^4)
C-Si-O	114.9	23.0218	-31.3993	24.9814
O-Si-O	110.7	70.3069	-6.9375	0.0
Si-O-Si	159.0	8.500	-13.4188	-4.1785
H-Si-O	107.4	57.664	-10.6506	4.6274
C-C-Si	120.0	61.0	-35.0	0.0
C-C-H	117.94	35.1558	-12.4682	0.0
C-C-C	118.9	61.0226	-34.9931	0.0
C-C-N	120.0	60.0	0.0	0.0
E_ϕ		V_1(kcal/mol)	V_2 (kcal/mol)	V_3 (kcal/mol)
Si-O-Si-O		-0.225	0.0	-0.010
Si-O-Si-H		0.0	0.0	-0.010
Si-O-Si-C		0.0	0.0	-0.010
H-C-C-H		0.0	2.35	0.0
Si-C-C-H		0.0	4.5	0.0
N-C-C- H		0.0	4.5	0.0
H-N-C-C		0.0	1.0	0.0
C_{ar}-C_{ar}-C_{ar}-C_{ar}		8.3667	1.2	0.0

E_{vdw}	r_{ij} (Å)	ε_{ij}(kcal/mol)
Si-Si	4.405	0.198
O-O	3.3	0.08
H-H	2.878	0.0230
C-C	3.915	0.068
N-N	3.83	0.096

Table 4: Partial Charges for atoms in the POSS molecules

			H(-Si)	H(-C)	H(-N)			
Molecule	q_{Si}	q_O	q_H	q_H	q_H	q_N	q_C	
OHS	0.808	-0.529	-0.0134					
OHS [45]	1.93	-1.10	-0.28					
OAPS	0.876	-0.538		0.174	0.258	-0.544	C(-SiC-)	-0.204
							C(-CH-)	-0.165
							C(-CN-)	0.1043

The LJ 6-12 potential and the electrostatic potential shown in Eq. (5) and (6), respectively are also used to model the interactions between PI atoms and POSS atoms. We used Lorentz-Berthelot [46] combining rules: $\sigma_{ij} = (\sigma_i + \sigma_j) / 2$ and $\varepsilon_{ij} = \sqrt{\varepsilon_i \varepsilon_j}$.

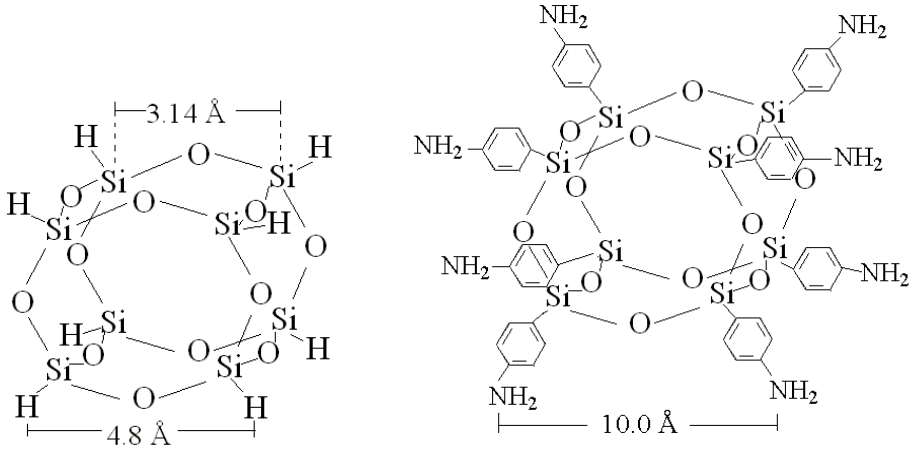

Figure 2: Structures of simulated POSS (a) Octahydrido silsesquioxanes (OHS), (b) Octaaminophenyl silsesquioxanes (OAPS).

3.2.2 Molecular dynamics details

All molecular dynamics (MD) simulations were performed using the LAMMPS [47] (Large-scale Atomic/Molecular Massively Parallel Simulator) program. To begin, a single PI chain was placed into a large simulation box at a very low density. To achieve the proper density, MD simulations in the NPT (constant number of particles, pressure, and temperature) ensemble were conducted at 1 atm and 800 K. The Nose/Hoover thermostat [48] and barostat [48] were used to control the temperature and pressure, respectively. The velocity Verlet integrator was used to integrate the equations of motion. The time step used was 0.5 fs for pure PI and OHS/PI systems, and 0.2 fs for OAPS/PI systems. Cutoff radii of 10 Å and 11 Å were used for LJ and Coulombic interactions, respectively for all simulations. A particle-particle/particle-mesh Ewald (PPPM) algorithm [49] was used for the long range Coulombic interactions. At 800 K, the single PI chain was relaxed until it formed a big coil in the simulation box. This relaxed PI chain was then used to start the simulation for each system. To make sure a system reached equilibrium, the simulation was initially conducted at 800K for more than 1 ns. A number of thermodynamic quantities were monitored during equilibration; if they remained stable for more than 0.5 ns, it was concluded that the system was equilibrated. The resulting box sizes of the equilibrated configurations for all the systems are shown in Table 5.

Table 5: Equilibrated box sizes for all systems at T = 800K

System	Equilibrated box sizes	Densities (g/cm^3)
1 Polyimide chain	30.56 Å x 33.34 Å x 27.79 Å	1.067
1 PI chain and 10.45 wt% OHS (5 OHS)	30.85 Å x 33.93 Å x 27.76 Å	1.161
1 PI chain and 5.96 wt% OAPS (1 OAPS)	34.92 Å x 32.01 Å x 26.19 Å	1.097
1 PI chain and 11.25 wt% OAPS (2 OAPS)	35.08 Å x 32.15 Å x 26.31 Å	1.147
1 PI chain and 20.23 wt% OAPS (4 OAPS)	42.60 Å x 31.24 Å x 25.56 Å	1.113

After equilibration, production runs were used to observe the properties of polymer and mixed-matrix materials, such as glass transition temperature. The glass transition temperature of a polymeric material can be determined by plotting specific volume versus temperature at constant pressure and noting where the slope changes. The specific volume as a function of temperature was obtained by performing simulations in the NPT ensemble with the temperature range of 400 K-800 K and pressure of 1 atm. Each system was first equilibrated at a temperature of 800K for about 1 ns, then the system was cooled to lower temperatures by decreasing the temperature by an increment of 25 K – 50 K. For temperatures lower than 800 K, the system was run for 500 ps. For all systems, specific volumes reached equilibrium after 100-250 ps, depending on the temperature.

In addition to the glass transition temperatures, we have also calculated the intermolecular radial distribution functions for PI-PI, POSS-POSS, POSS-PI. The production runs for these cases considered larger systems which contain 4 PI chains. This large system was created by first cooling the system obtained from the glass transition temperature studies from 400 K to 325 K with 25 K intervals, and then from 325 K, it was again cooled to 308 K. At each temperature, the simulations were run for 500 ps. Then, at 308 K, we replicated twice of the number of atoms in *y* and *z* directions, and ran the simulation for 2 ns in the NPT ensemble. To ensure that the structure that we obtained in the production run is in equilibrium, we compared the rdf plots after the simulation runs of 1 ns, 1.5 ns, and 2 ns. If the difference was smaller than 5%, then the structure was concluded to be at equilibrium. For the 20.23 wt% OAPS system, we found that the radial distribution function based on POSS to POSS did not reach equilibrium after the 2

ns run; another 1.5 ns of simulation time was needed to get an equilibrated radial distribution function.

We also calculated mean square displacement for PI and POSS. This calculation was done at 650 K. The production runs for this case considered large systems as well. The equilibrated system at 650 K obtained from glass transition temperature observation was used as the initial configuration. We then replicated twice of the number of atoms in *y* and *z* directions, and ran the simulation for about 1.5 ns in the NPT ensemble.

Table 6: Equilibrated box sizes for large systems at T = 308K

System	Box sizes
4 Polyimide chain	26.84 Å x 58.57 Å x 48.81 Å
4 PI chain and 10.45 wt% OHS (20 OHS)	27.76 Å x 61.07 Å x 49.97 Å
4 PI chain and 5.96 wt% OAPS (4 OAPS)	31.01 Å x 56.85 Å x 46.52 Å
4 PI chain and 11.25 wt% OAPS (8 OAPS)	31.69 Å x 58.10 Å x 47.54 Å
4 PI chain and 20.23 wt% OAPS (16 OAPS)	38.47 Å x 56.43 Å x 46.17 Å

3.3 Results and discussion

3.3.1 Glass transition temperature

NPT molecular dynamics simulations were conducted at 1 atm to calculate the volume – temperature properties of the pure PI and PI-POSS blends. The uncertainty for the specific volume is in the range of 0.01-0.04 cm^3/g, in terms of the standard error calculated for the specific volume during the production run. The specific volume versus temperature plots are shown in Figure 3 for PI, a blend of PI and 10.45 wt% OHS, and a blend of PI and 20.23 wt% OAPS. The temperature at which the slope changes on the specific volume - temperature plot represents the glass transition temperature (T_g) [16], [50]. An arrow indicates the location of T_g. Simulations were also performed for a blend with 5.96 and 11.25 wt% OAPS. The standard error for the T_g calculation is ~ 9-15 K for

different systems, which is based on the errors associated with the two least-squares linear regression fits of the specific volume versus temperature.

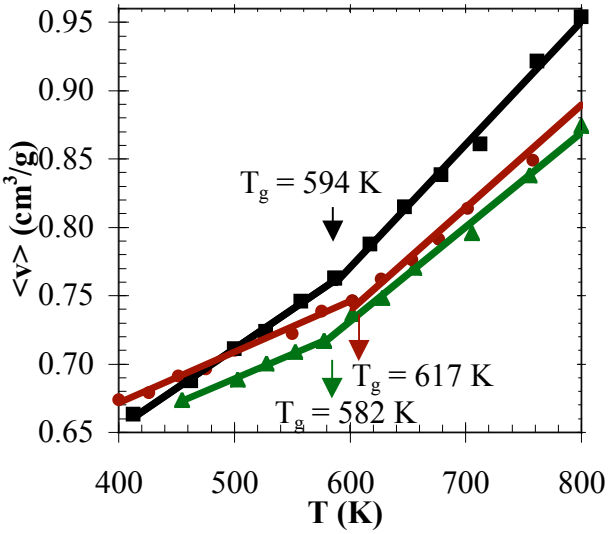

Figure 3: Specific volume (<v>) vs. temperature for pure PI (black), PI and 20.23 wt% OAPS (dark red), PI and 10.45 wt% OHS (green) at 1 atm obtained from NPT dynamics. The symbols indicate the state points calculated with MD simulation. The lines shown are least-squares linear regression fits through the data. The arrow indicates the position of the T_g from MD simulation.

The glass transition temperatures and specific volumes for the pure PI and POSS-PI blends obtained from the simulations and experiments [31] are summarized in Table 7. The simulated glass transition temperatures are about 4 % higher than the experimental values. The specific volumes for each system are reported at 300 K. For the pure PI and OAPS systems, the specific volumes obtained from the simulation are about 10 % smaller than the experimental results. The experimental results shown in Table 7 were obtained using PI with the number-average molecular weight of 47152, which is about twice more than the length of the PI chain considered in the current simulation work. In the literature [51], [52], it has been shown that by varying the number of repeat units, the glass transition temperature of a polymer will shift. Additionally, the cooling rates used in the

simulation are much higher (of order 10^{10} K/s) than experimental cooling rates. This is necessary due to computational limitations, which restrict the simulation to timescales on the order of picoseconds [53]. It is known that a higher cooling rate may shift the glass transition temperature to a higher value [53], [54]. Therefore, in this comparison, the simulation results are expected to agree qualitatively but not quantitatively to the experimental results.

The incorporation of OAPS has caused an increase of the T_g. Qualitatively, the model correctly reproduces the experimentally observed effect of increased OAPS loading up to 11 wt% on T_g. Namely, that the glass transition temperature gradually increases up to that weight percent of OAPS [31] and then remains constant beyond 10 wt% of OAPS, up to 30 wt% [31]. While simulation results show a slight decrease of the T_g after the addition of 20 wt% OAPS, this decrease is within the bounds of uncertainty and not significant.

Table 7: Glass transition temperatures and specific volumes for POSS-PI blends at 1 atm.

	Wt % POSS, MD	**T_g(K), MD**	**<v>[a] (cm^3/g), MD**
MD Simulation Results	0	594	0.627
	5.96 OAPS	606	0.638
	11.25 OAPS	622	0.640
	20.23 OAPS	617	0.644
	10.45 OHS	582	0.631
	Wt % POSS, expt.	**T_g (K) [b], expt.**	**<v> [a,c] (cm^3/g), expt.**
Experimental Results	0	570	0.725
	5 OAPS	582	0.715
	10 OAPS	591	0.713
	20 OAPS	592	0.714
	10 OHS	-	-

[a]Specific volumes at 300 K.
[b]Experimental data from Ref 31.
[c]Iyer and Coleman, personal communication.

The T_g value for system containing 10.45 wt% OHS blended with PI is lower than the T_g value for the pure PI. This reduction in T_g is expected because OHS (hydrogen-functionalized POSS) is known to be incompatible with PI. We are not aware of experimental data for OHS/PI blends. Similar reduction in T_g was observed for octaphenyl-POSS (OPS)/PI blends in experiments by Iyer and Coleman [31]. They observed unfavorable interactions between OPS and PI which suggested the incompatibility of these two species.

To check the effects of system size on the glass transition temperature determination, we compared the specific volume obtained from the small systems (containing 1 PI chain) at 308 K to the specific volume obtained from the large systems (containing 4 PI chains) at 308 K. The results are comparable with the difference of the values of less than 1 %.

3.3.2 Radial distribution functions

The radial distribution function (rdf), g(r) provides more understanding of the POSS and polymer packing details. As mentioned before, the simulations conducted to calculate the rdfs contained 4 PI chains. These systems were larger to obtain better statistics for the rdf analysis. In this section, we present rdfs for PI-PI, POSS-POSS, and POSS-PI. Figure 4 shows the intermolecular packing, g(r) based on all atom centers of PI to PI in the systems. The g(r) has a lower value with the incorporation of 5.96 and 11.25 wt% OAPS compared to the one with 0 wt% POSS. This indicates that with the incorporation of OAPS up to 11.25 wt%, the presence of OAPS decreased the density of contacts between PI to PI. On the other hand, the incorporation of 20.23 wt% OAPS shows that the density of contacts between PI to PI is the same as for 0 wt% POSS. This

indicates that the incorporation of 20.23 wt% OAPS may have caused the PI polymers to start to cluster together and phase separate from the POSS. The g(r) for 10.45 wt% OHS also suggests that the PI has phase separated from the POSS.

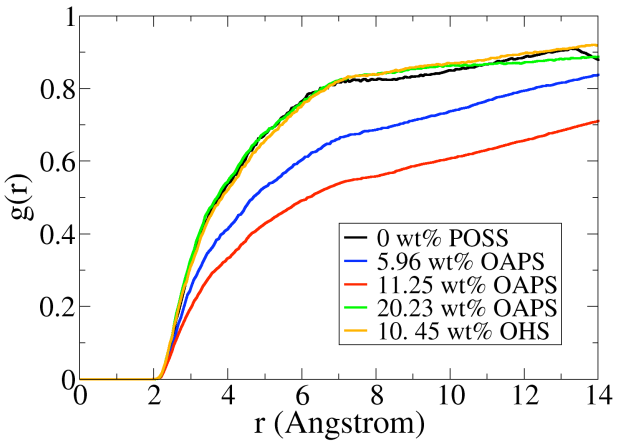

Figure 4: Radial distribution function based on all atom of PI to all atom of PI for system with 0 wt% POSS, 10.45 wt% OHS, 5.96, 11.25, and 20.23 wt% OAPS at 308K.

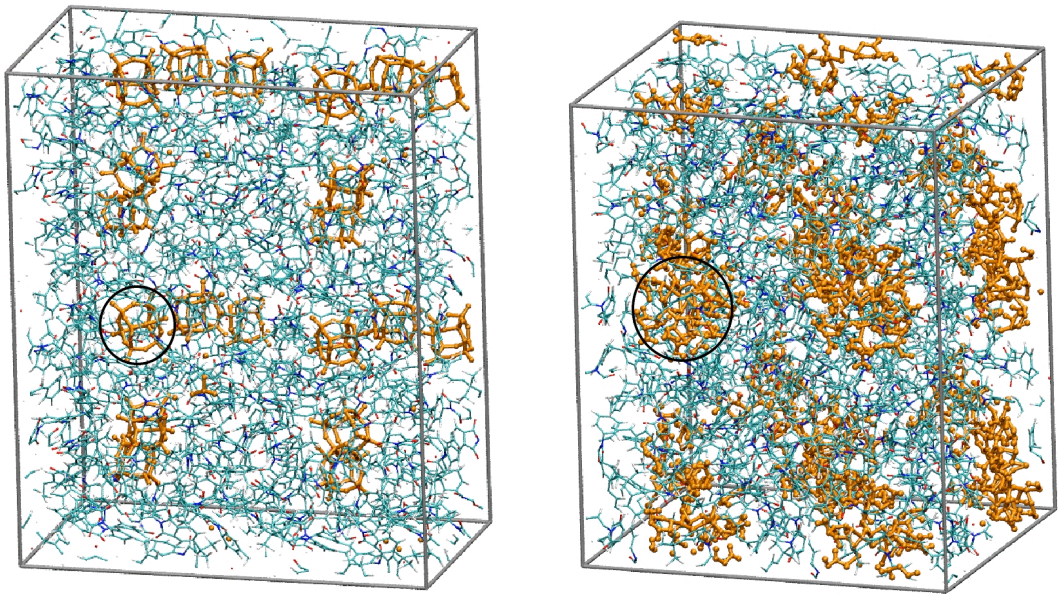

(a) (b)

Figure 5: Snapshot of POSS molecules (orange) and PI (a) 10.45 wt% OHS/PI blends at 308K, (b) 20.23 wt% OAPS/PI blends at 308K. For clarity, a single POSS molecule is circled in each snapshot. Snapshots generated with Visual Molecular Dynamics (VMD) [55]

The intermolecular packing of POSS to POSS based on the Si and O atoms in polymeric system is shown in Figures 6 and 7. Figure 6 compares the g(r) for system with 10.45 wt% OHS to the g(r) for system with 11.25 wt% OAPS at T = 308K. The g(r) data for OHS indicate that there are distinct peaks at around r = 4.0, 6.0, and 7.5 Å. These peaks are direct evidence that there is a specific organization of the neighboring OHS molecules in PI system, indicating that aggregation of OHS has occurred. The aggregation can also be seen in the snapshot shown in Figure 5(a). It has been stated that POSS molecules tend to crystallize at room temperature [29], [56]. Zheng *et al.* [56] observed that aggregation and crystallization occurred for octaisobutyl-POSS within polysiloxane elastomer. However, the short simulation time duration used here makes it impossible to observe any tendency of spontaneous crystallization of POSS. On the other hand, the g(r) data for 11.25 wt% showed that the OAPS-OAPS contacts started to show only at the distance of 5.5 Å. There are no distinct peaks shown in the plot, which means a weak, liquid like ordering structure of OAPS molecules. Figure 7 shows the comparison of the rdf plots for POSS with different loadings of OAPS. The data from 5.96 wt% OAPS is not shown because the OAPS molecules are more dilute in the PI system, and therefore did not exhibit any aggregation on the time scale of the simulation. For the 11.25 and 20.23 wt% OAPS, both plots indicate featureless coordination of OAPS within the PI system, which means a good dispersion of OAPS. This can be also seen in the snapshot shown in Fig. 5(b).

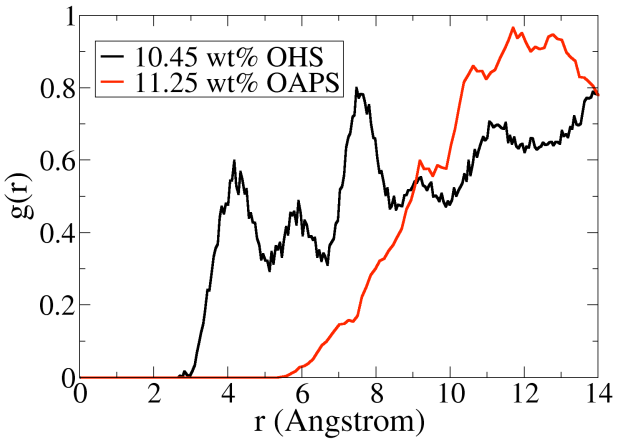

Figure 6: Radial distribution function based on POSS to POSS (Si and O atom types) for system with 10.45 wt% OHS and 11.25 wt% OAPS at 308K.

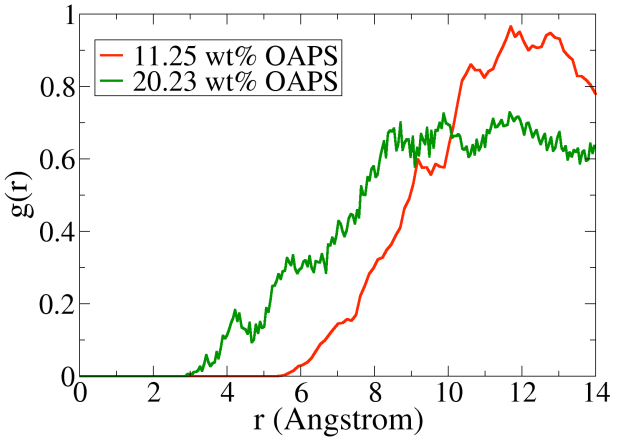

Figure 7: Radial distribution function based on POSS to POSS (Si and O atom types) for system with 11.25 wt% OAPS and 20.23 wt% OAPS at 308K.

Figure 8 shows the intermolecular packing of the PI polymer chains around the POSS at T = 308K. The rdf shown is based on all atom polyimide chain to all atom POSS. The plot shows some diffuse peaks for system with 10.45 wt% OHS at $r \sim 4$ Å and 8 Å, which means that the packing of PI to OHS is more structured than the packing of PI to OAPS. The geometry of the POSS cage, composed of Si and O atoms is highly constrained and only capable of small deformation [16]. Therefore, the main difference between OAPS and OHS is in the way that the substituents (aminophenyl groups or hydrogen atoms) pack around the POSS cage. Since there are only hydrogen atoms as the

functional groups on the OHS molecule, OHS can pack more compactly, which allows the polymer chains to approach closer to the OHS. The plot for 10.45 wt% OHS system shows the highest g(r) at almost all distances less than 9.7 Å. This means that the density of PI-OHS contacts is higher compared to density of PI-OAPS contacts. For different loadings of OAPS, the highest density of PI-OAPS contacts occurred for the system with 20.23 wt% OAPS. There is not much difference of how the PI chain packed around the POSS molecules for low loading (5.96 wt% and 11.25 wt%) of OAPS.

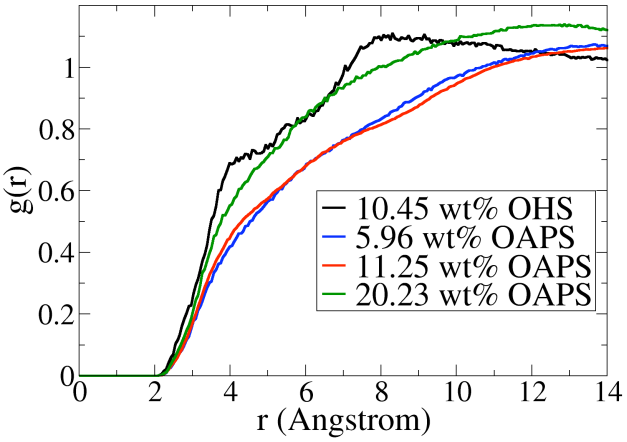

Figure 8: Radial distribution function based on all-atom POSS to all-atom polyimide for system with 10.45 wt% OHS, 5.96 wt% OAPS, 11.25 wt% OAPS, and 20.23 wt% OAPS at 308K.

Experimental studies have shown that the increase of T_g due to the incorporation of POSS can be because of two aspects: (i) when POSS increases the interaction contacts between POSS to polymer chain [31], [57], [58], [59] i.e., a good dispersion of POSS in the polymer system, and (ii) when the relatively rigid POSS molecules retard the motion of the polymer [31], [57], [60]. Iyer *et al.* [31] also noted that T_g may decrease if phase separation takes place. From the radial distribution functions based on POSS to POSS, aggregation occurred for OHS molecules. In addition, Fig. 4 has shown there is no effect on PI to PI contacts after the addition of OHS molecules in the system. This means that

the PI polymer chains were still clustering together. These two facts indicate that phase separation might have occurred and caused the lower T_g for this blend. The rdfs for OAPS systems based on POSS to POSS showed that OAPS molecules do not have the tendency to aggregate. Fig. 4 has also shown a decrease of PI to PI interaction contact for low loading (5.96 wt% and 11.25 wt%) of OAPS. These indicate that OAPS molecules were well dispersed in the systems. Our simulation results have shown there was a gradual increase in T_g as the OAPS loading increased up to 11.25 wt. In the following section, the effect of POSS on the mobility of the PI chain will be discussed.

3.3.3 Mobility of PI and POSS

To observe the mobility of PI chains in the nanocomposite materials, the mean square displacements (MSD) were calculated at a temperature above the glass transition temperature, 650 K. Figure 9 shows the MSD plots for PI for all cases. The MSD are calculated based on the center of mass of each polyimide chain and averaged over the 4 chains. The presence of POSS molecules on PI polymeric system was expected to affect the mobility of the polymer chain [31]. The mobility of PI chain decreased with the incorporation of OAPS, on the other hand, the mobility increased slightly with the incorporation of OHS. These observations agree with the glass transition temperature results, which showed an increase of the T_g after the incorporation of OAPS, and a decrease of the T_g after the incorporation of OHS. The least steep slope of MSD for PI is found for 11.25 wt% OAPS system. This indicates that the mobility of the PI chains were the slowest for this system.

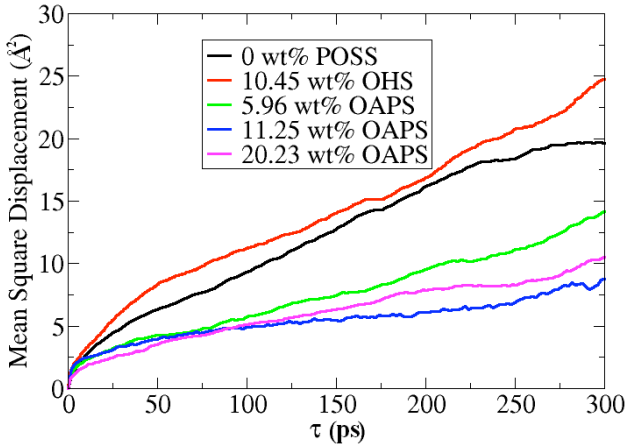

Figure 9: Mean square displacement of the PI chains for all systems at T = 308K

Besides the mobility of PI chains, we have also observed the mobility of POSS molecules at T=650 K. Figure 10 shows the mean square displacement plot for POSS molecules in PI polymer chains. The MSD calculations consider multiple origins separated by 2.0 ps and they are averaged over all POSS molecules in each system. It is shown that the MSD for OHS molecules is higher compared to the MSD for OAPS at all times. The smaller size and the compact structure of OHS allow it to move more in the PI system compared to the OAPS. The aminophenyl groups in OAPS decrease the motion of the POSS molecules in the polymeric matrix. The slope of the MSD plot for 11.25 wt% system is the least steep one. This means that OAPS for this system has the slowest motion compared to the other systems. Our glass transition temperature results showed that the T_g for system with 11.25 wt% OAPS was the highest. These observations support our glass transition temperature results discussed earlier. If the addition of POSS molecules retards the motion of the species in a nanocomposite, the glass transition temperature will increase. In addition to that, the aminophenyl group has been known to improve the compatibility of POSS to the PI chain [31]. The compatibility of these two

species will make them interact more favorable, and therefore retard the motion of both species.

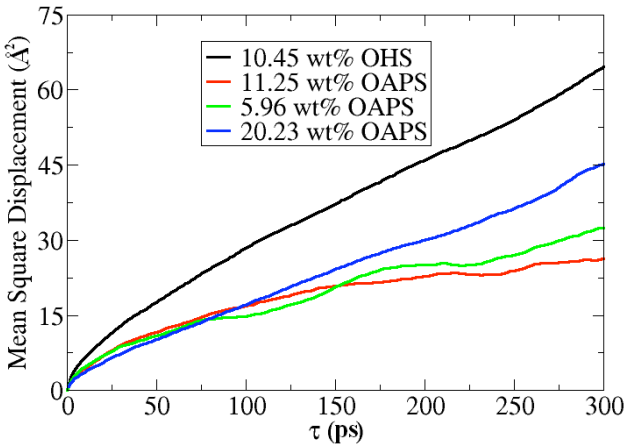

Figure 10: Mean square displacement of the POSS molecules for system with 5.96 wt% OAPS,11.25 wt% OAPS, and 20.23 wt% OAPS at T=308K

3.4 Conclusions

The effect of incorporating POSS to the polyimide polymer matrix has been explored with atomistic molecular dynamics simulations. The specific volume versus temperature plots were obtained from simulations to determine the glass transition temperatures. The glass transition temperatures obtained from simulations agree qualitatively to the results obtained from experiment. The blending of OAPS into the PI matrix showed an increase of the glass transition temperatures. An increase of up to 11.25 wt % of OAPS increases the glass transition temperatures of the materials. On the other hand, the blending of OHS into the PI matrix showed a decrease of the glass transition temperature.

From the radial distribution functions calculations, it was shown that the density of PI-OHS contacts is higher compared to the density of PI-OAPS contacts. PI chains packed more efficiently around OHS than around OAPS. This is due to the more compact structure and the much denser molecule of OHS compared to OAPS. The OHS molecules

arranged in a more ordered fashion compared to the OAPS molecules in nanocomposite materials. Radial distribution functions plots also show the liquid like ordering structure of OAPS molecules in the polymeric system.

The mobility of PI chains and POSS molecules was observed by the mean squared displacements. The incorporation of OAPS has reduced the mobility of polyimide. However, the incorporation of OHS has slightly increased the mobility of polyimide chains.

Our simulation results have shown the behavior of POSS in PI polymer matrix. PI is a rigid polymer. For future study, a flexible backbone polymer, poly(dimethylsiloxane), PDMS, will be considered. This flexible polymer is expected to allow more loading of POSS. Our current results have shown that the incorporation of OAPS increased the glass transition temperature of the nanocomposite materials. Another motivation will be also to consider the PI-PDMS copolymer. This copolymer will combine the advantage of PI (high glass transition temperature) and the flexibility of PDMS which may then lead to a copolymer that can withstand elevated temperature and therefore can be used for applications, such as membranes for gas separation.

Acknowledgments

This work was supported by the Department of Chemical and Biological Engineering at Iowa State University. The computational work was performed at the ISU High Performance Computing facility.

References

[1] Paul DR, and Yampol'skii YP. Polymer Gas Separation Membranes: Introduction and Perspective; CRC Press, 1994.
[2]Zimmerman CM, Singh A, Koros WJ. *J Membr Sci* 1997, 137: 145-154.
[3] Dodiuk H, Rios PF, Dotan A, Keniq S. *Pol Adv Tech* 2007, 18: 746-750.
[4] Oaten M, Choudhury NR. *Macromolecules* 2005, 38: 6392-6401.
[5] Devaux E, Rochery M, Bourbiqot S. *Fire and Materials* 2002, 26: 149-154.
[6] Laine RM. *J Mater Chem* 2005, 15: 3725.
[7] Peng Y, McCabe C. *Mol Phys* 2007, 105: 261.
[8] Ionescu TC, Qi F, McCabe C, Striolo A, Kieffer J, Cummings PT. *J Phys Chem B* 2006, 110: 2502.
[9] Pielichowski K, Njuguna J, Janowski B, Pielichowski J. *Adv Polym Sci* 2006, 201: 225-296.
[10] Striolo A, McCabe C, Cummings PT. *J Phys Chem B* 2005, 109: 14300.
[11] Agaskar PA. *Inorg Chem* 1991, 30: 2707.
[12] Laine RM, Zhang C, Sellinger A, Viculis L. *Appl Organometal Chem* 1998, 12: 715.
[13] Striolo A, McCabe C, Cummings PT. *Macromolecules* 2005, 38 (21): 8950-8959.
[14] Striolo A, McCabe C, Cummings PT, Chan ER, Glotzer SC. *J Phys Chem B* 2007, 111 (42): 12248-12256.
[15] Striolo A, McCabe C, Cummings PT. *J Chem Phys* 2006, 125: 104904.
[16] Bharadwaj RK, Berry RJ, Farmer BL. *Polymer* 2000, 41: 7209.
[17] Lichtenhan JD. *Comm. Inorg Chem* 1995, 17: 115-130.
[18] Mark JE. *Macromol Symp* 2003, 201: 77-83.
[19] Li GZ, Wang LC, Ni HL, Pittman Jr. CU. *J Inorg Organomet Pol* 2001, 11: 123-154.
[20] Schwab JJ, Lichtenhan JD. *Appl Organometal Chem* 1998, 12: 707-713.
[21] Lee YJ, Huang JM, Kuo SW, Lu JS, Chang FC. *Polymer* 2005, 46: 173-181.
[22] Leu CM, Chang YT, Wei KH. *Chemistry of Materials* 2003, 15: 3721-3727.
[23] Chen YW, Kang ET. *Materials Letters* 2004, 58: 3716-3719.
[24] Mather PT, Jeon HG, Romo-Uribe A. *Macromolecules* 1999, 32: 1194-1203.
[25] Lichtenhan JD, Otonari YA, Carr MJ. *Macromolecules* 1995, 28: 8435-8437.
[26] Romo-Uribe A, Mather PT, Haddad TS, Lichtenhan JD. *J Poly Sci B Polym Phys* 1998, 36: 1857-1872.
[27] Haddad TS, Lichtenhan JD. *Macromolecules* 1996, 29: 7302.
[28] Kim KM, Keum DK, Chujo Y. *Macromolecules* 2003, 36: 867-875.
[29] Liu L, Tian M, Zhang W, Zhang LQ, Mark JE. *Polymer* 2007, 48: 3201-3212.
[30] Liu L, Hu Y, Song L, Nazare S, He SQ, Hull R. *J Mat Sci* 2007, 42: 4325-4333.
[31] Iyer P, Coleman MR. *J Appl Pol Sci* 2008, Vol. 108: 2691-2699.
[32] Xu H, Kuo JW, Lee JS, Chang FC. *Macromolecules* 2002, 35: 8788-8793.
[33] Fu BX, Hsiao BS, Pagoda S, Stephens P, White H, Rafailovich M, Sokolov J, Mather PT, Jeon HG, Phillips S, Lichtenhan J, Schwab J. *Polymer* 2001, 42: 599.
[34] Zheng L, Farris RJ, Coughlin EB. *Macromolecules* 2001, 34: 8034-8039.
[35] Capaldi FM, Rutledge GC, Boyce MC. *Macromolecules* 2005, 38: 6700-6709.
[36] Patel RR, Mohanraj R, Pittman JR. CU. *J Polym Sci: Part B: Polym Phys* 2006, Vol. 44: 234-248.

[37] Chan ER, Striolo A, McCabe C, Cummings PT, Glotzer SC. *J Chem Phys* 2007, 127:114102.
[38] Clark M, Cramer III RD, and Opdenbosch NV. *J Comp Chem* 1989, 10: 982-1012.
[39] Pinel E, Brown D, Bas C, Mercier R, Alberola ND, Neyertz S. *Macromolecules* 2002, 35: 10198-10209.
[40] Qi D, Hinkley J, He G. *Modelling Simul Mater Sci Eng* 2005, 13: 493-507.
[41] Schmidt MW, Baldridge KK, Boatz JA, Jensen JH, Koseki S, Matsunaga N, Gordon MS, Ngugen KA, Su S, Windus TL, Elbert ST, Montgomery J, Dupuis M. *J Comput Chem* 1993, 14: 1347.
[42] (a)Hehre WJ, Ditchfield R, Pople JA. *J Phys Chem* 1972, 56: 2257. (b)Francl MM, Pietro WJ, Hehre WJ, Binkley JS, Gordon MS, Defrees DJ, Pople JA. *J Chem Phys* 1982, 77: 3654. (c)Clark T, Chandrasekhar J, Spitznagel GW, Schleyer PVR. *J Comput Chem* 1983, 4: 294. (d)Frisch, M. J.; Pople, J. A.; Binkley, J. S. *J Chem Phys* 1984, 80: 3265. (e)Okuno, Y. *J Chem Phys* 1996, 105: 5817.
[43]Pigache A, Cieplak P, and Dupradeau FY, Automatic and highly reproducible RESP and ESP charge derivation: Application to the development of programs RED and X RED, 227th ACS National Meeting, Anaheim, CA, USA, March 28 - April 1, 2004.
[44] Sun H. *J Phys Chem B* 1998, 102: 7338-7364.
[45] Li HC, Lee CY, McCabe C, Striolo A, Neurock M. *J Phys Chem A* 2007, 111 (18): 3577-3584.
[46]Allen MP, and Tildesley DJ. *Computer Simulation of Liquids* (Clarendon, Oxford, 1987).

[47] Plimpton SJ. *J Comp Phys*1995, 117: 1-19.
[48] Frenkel D, Smit B. *Understanding Molecular Simulation* 2002, 2nd ed.
[49] Hockney R, Eastwood J. *Computer Simulations Using Particle*, Adam Hilger: New York, 1988.
[50] Nicholson JW. *The Chemistry of Polymers* 2006, 3rd Ed.
[51] Fox TG, and Flory PJ. *Journal of Applied Physics* 1950, 21, pp. 581–591.
[52] Zhang J, Liang Y, Yan JZ, Lou JZ. *Polymer* 2007, 48: 4900-4905.
[53] Soldera A, Grohens Y. *Macromolecules* **2001**, 35 (3), 722-726.
[54] Bizet S, Galy J, Gerard JF. *Polymer* **2006**, 47:8219-8227.
[55] Humphrey W, Dalke A, and Schulten K. "VMD-Visual Molecular Dynamics", *J Molec Graphics*, 1996, vol. 14, pp. 33-38.
[56] Zheng L, Waddon AJ, Farris RJ, Coughlin EB. *Macromolecules* 2002, 35: 2375.
[57] Huang JC, He CB, Xiao Y, Mya KY, Dai J, Siow YP. *Polymer* 2003, 44: 4491-4499.
[58] Wahab MA, Kim I, Ha CS. *Polymer* 2003, 44: 4705.
[59] Xiong M, You B, Shuxue Z, Limin W. *Polymer* 2004, 45: 2967.
[60] Lee A. *Mat Res Soc Symp Proc* 1999, Vol. 576: 343-350.

CHAPTER 4 MOLECULAR DYNAMICS SIMULATION OF POLYMER-INORGANIC NANOCOMPOSITES BASED ON POLY(DIMETHYL SILOXANE) (PDMS)/OCTAAMINOPHENYL SILSESQUIOXANE (OAPS) AND POLYIMIDE-PDMS/OAPS

Abstract

Nanocomposite materials containing polymer and octaaminophenyl silsesquioxanes (OAPS) are studied with atomistic molecular dynamics simulation. Two types of polymer are considered, either poly(dimethyl siloxane) (PDMS) or polyimide (PI)-PDMS. The blending of OAPS into both polymer matrices showed an increase of the glass transition temperatures. Radial distribution functions are examined to show how the polymers and OAPS species pack in the nanocomposite materials. The mobility of PDMS, PI-PDMS chains and OAPS molecules was observed by calculating the mean squared displacements. The incorporation of OAPS is shown to reduce the mobility of both PDMS and PI-PDMS polymer chains.

4.1 Introduction

Polymer-inorganic nanocomposites, also known as mixed matrix materials, have been used widely in membrane applications [1], [2]. A mixed matrix material incorporates inorganic fillers within a polymer matrix. Mixed matrix materials combine the advantages of polymeric materials (processability, cost effectiveness, and good transport properties) and inorganic materials (thermal stability, rigidity and high selectivity) into a single material. The inorganic fillers can improve the mechanical and structural properties of the polymer [3], [4], [5]. Frequently the addition of an inorganic filler increases the strength and heat resistance of the polymer matrix, and hence, makes

possible the use of polymer-based materials under high-temperature operating conditions such as in gas separation processes. In addition to that, the rigid inorganic filler can reduce the mobility of the polymer chains, and therefore improve the membrane's selectivity at elevated temperature.

One important property to observe in designing a mixed matrix material is the glass transition temperature. To be able to obtain a membrane that can withstand a high temperature, a material with a high glass transition temperature is desired. The presence of the inorganic fillers is expected to increase the glass transition temperature of the mixed matrix material. If there is a good contact between polymer matrix and the surface of the inorganic filler, the glass transition temperature of the mixed matrix material will increase. On the other hand, if there is a poor contact between those two materials, glass transition temperature will decrease. The poor contact between the polymer and the inorganic filler may also lead to a macroscopic void that will result in a nonselective pathway of gas transport for the membrane. Therefore, a proper selection of the polymer matrix and the inorganic filler is important to be able to design a robust membrane for promising gas separation properties.

There are several types of polymers that have been used in designing mixed matrix membranes, such as glassy polymers [6], [7], flexible polymers [8], [9], [10], [11], and copolymers that contain both glassy and flexible segments [12]. Glassy polymers have a high glass transition temperature. However, due to the rigidity of this class of polymer, it often makes poor contact with the rigid inorganic filler. The presence of poor contacts may then lead to interphase voids. In contrast to glassy polymers, a rubbery/flexible polymer maintains good contact with the inorganic fillers, which then

results in a significant increase in selectivity for the membrane material at the interface of the two materials. This is true especially with high loading of the fillers [7], [9], [10]. However, a rubbery polymer lacks mechanical stability at high temperature compared to a glassy polymer [7].

A block copolymer composed of both flexible and rigid segments has also been used in making mixed matrix membranes [12]. The flexible segment of the block copolymer promotes good contact of the polymer with the fillers, and the rigid segment provides a high selectivity and thermal stability to the membrane. Pechar *et al.* [12] designed a mixed matrix membrane using polydimethylsiloxane (PDMS)-polyimide (4,4'-(hexafluoroisopropylidene)diphthalic anhydride, 6FDA-4,4'-(hexafluoroisopropylidene)dianiline, 6FpDA) block copolymer with zeolite fillers. Their observations showed no evidence of the polymer being separated from the zeolites, which suggests a good dispersion of the two components. They have also shown an increase of the membrane permeability for He, CO_2, O_2, N_2, and CH_4 gases with the use of 22 and 41 wt% PDMS in the block copolymer.

As mentioned earlier, a proper choice of the fillers is also an important thing to consider in designing a mixed matrix material. Polyhedral oligomeric silsesquioxanes (POSS) are one of the inorganic fillers that have been used. POSS has the chemical composition of $(RSiO_{1.5})_n$ with R as an organic functional group. The possibility to synthesize POSS with different functional groups results in many potential application areas for POSS-based materials, for example, as additives to paints and coatings, [13], [14], [15] as well as in packaging materials and advanced plastics where POSS enhances temperature resistance [16], [17], [18], [19]. There are different ways to incorporate

POSS in the polymer matrix, such as by physically blending the POSS molecules with the polymer [20], by introducing them as pendant groups on the polymer chain [21], or by covalent binding within the polymer backbone [21], [22]. The incorporation of POSS molecules into a polymer results in improved material properties such as increased thermal stability, increased glass transition temperature, improved heat resistance, and reduction in flammability and heat evolution [13], [14], [19], [23], [24].

The number of studies about the incorporation of POSS in polymeric materials has grown, however, there is still a lot more to understand concerning the effect of POSS on the thermal properties of the materials [25], [26] and whether POSS molecules disperse uniformly within the polymer or form aggregates [27], [28], [29]. In the last decade, molecular simulations have contributed to our knowledge about the fundamental interactions between polymer and POSS species.

In earlier work [30] we considered POSS blended with a glassy polymer, polyimide (6FDA-MDA). We used molecular dynamics simulation to observe the effect of the incorporation of octahydrido silsesquioxane (OHS) and octaaminophenyl silsesquioxane (OAPS) in the polyimide matrix to the glass transition temperature of the material. Our modeling results have shown a decrease of the glass transition temperature with the incorporation of OHS in polyimide (PI) matrix and an increase of the T_g with the incorporation of OAPS in the PI matrix.

In this work, we provide a detailed molecular dynamics simulation study of two nanocomposites: i) OAPS blended with a flexible polymer, PDMS and ii) OAPS blended with a glassy-flexible copolymer (2,2-bis(3,4-dicarboxyphenyl)-hexafluoropropane dianhydride (6FDA)/4,4'-diaminediphenylmethane (MDA) polyimide (PI)-PDMS). The

paper is organized as follows: in Section 2, a detailed explanation of the force fields used in this work is provided and the molecular dynamics simulation method is explained; in Section 3, the simulation results are discussed; and in Section 4, a summary of the findings is provided.

4.2 Molecular Models and Simulation Methods

4.2.1 Molecular models

The systems studied consist of PDMS, octaaminophenyl silsesquioxane (OAPS)/PDMS blends, PI(6FDA-MDA)-PDMS, and OAPS/PI-PDMS blends. The chemical structures for the PDMS repeat unit and PI-PDMS repeat unit are shown in Figure 1a and 1b, respectively. The molecular weight of the PDMS was 2473.04 g/mol, corresponding to a n = 30 monomer chain. The molecular weight of the PI-PDMS was 46868.3 g/mol, corresponding to x = 4, y = 1, and n = 30 monomers. One monomer of the copolymer chain contains about 24 wt% of PDMS. The chemical structure for OAPS is shown in Figure 2, with the cube's edge length (N to N) of about 10 Å.

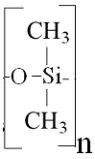

(a)

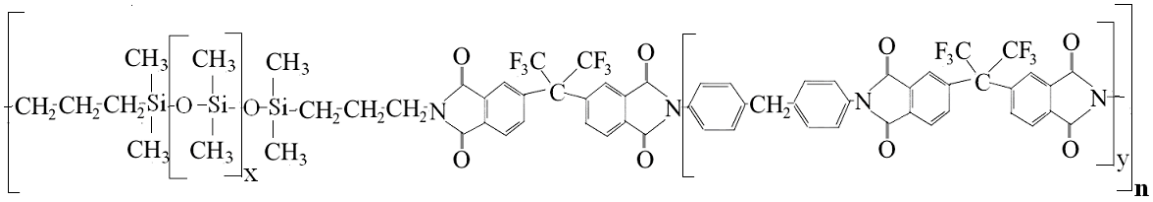

(b)

Figure 1: (a) Repeat unit of the PDMS polymer chain (b) Repeat unit of the 6FDA-MDA-PDMS polymer chain

The united atom (UA) model, in which hydrogen atoms are modeled implicitly, was used for both PDMS and PI-PDMS polymers. A hybrid/UA developed by Frischknecht *et al.* was employed for PDMS. This force field accounts for bond stretching (E_b), angle bending (E_θ), and torsional potential (E_ϕ). The harmonic functional form of bond stretching and angle bending are defined in Equation (1) and (2), respectively.

$$E_b = k_b\left(d_{ij} - d_{ij}^o\right)^2 \tag{1}$$

$$E_\theta = k_\theta\,(\theta - \theta_o)^2 \tag{2}$$

where d_{ij} is the actual bond length, d_{ij}^0 is the equilibrium bond length, θ is the actual bond angle, θ_0 is the equilibrium bond angle, k_b, k_θ are the constants. The Si-CH_2-CH_2 bond-angle potentials are described by following the COMPASS [31] formalism which is shown in Eq. (3). This form was also used by Striolo *et al.* [5] to describe the similar bond-angle potential.

$$E_\theta = k_\theta^I\,(\theta - \theta_o)^2 + k_\theta^{II}\,(\theta - \theta_o)^3 + k_\theta^{III}\,(\theta - \theta_o)^4 \tag{3}$$

The torsional-angle potential is expressed by

$$E_\phi = c_1\left[\left(1 + \cos(\phi)\right)\right] + c_2\left[\left(1 - \cos(2\phi)\right)\right] + c_3\left[\left(1 + \cos(3\phi)\right)\right] \tag{4}$$

where ϕ is the actual value of the torsional angle, c_1, c_2, and c_3 are the constants. The nonbonded interaction terms accounted for hybrid/UA model include the van der Waals and electrostatic potentials. The Lennard Jones (LJ) 12-6 function, shown in Eq. (5) was used to model the van der Waals interactions. We used Lorentz-Berthelot [32] mixing rules: $\sigma_{ij} = (\sigma_i + \sigma_j) / 2$ and $\varepsilon_{ij} = \sqrt{\varepsilon_i \varepsilon_j}$. For Si and O atoms, the LJ 9-6, shown in Eq. (6) was used. The mixing rules for Si-O potential were shown in Eq. (7) and (8).

$$u_{ij}(r) = 4\varepsilon_{ij}\left[\left(\frac{\sigma_{ij}}{r_{ij}}\right)^{12} - \left(\frac{\sigma_{ij}}{r_{ij}}\right)^{6}\right] \tag{5}$$

$$u_{ij} = \varepsilon_{ij}\left\{2\left[\frac{\sigma_{ij}}{r}\right]^{9} - 3\left[\frac{\sigma_{ij}}{r}\right]^{6}\right\},\ i \text{ and } j = \{\text{Si, O}\} \tag{6}$$

$$\sigma_{SiO} = \left(\frac{\sigma_{Si}^{6} + \sigma_{O}^{6}}{2}\right)^{1/6} \tag{7}$$

$$\varepsilon_{SiO} = \left(\frac{2\sigma_{Si}^{3}\sigma_{O}^{3}\sqrt{\varepsilon_{Si}\varepsilon_{O}}}{\sigma_{Si}^{6} + \sigma_{O}^{6}}\right) \tag{8}$$

In Eq. (5), (6), (7), and (8), ε_{ij} is the Lennard-Jones well-depth, σ_{ij} is the Lennard-Jones diameter, and r_{ij} is the distance between atom i and j. The electrostatic potential is expressed by

$$E_{coul} = \sum_{i,j}\frac{q_i q_j}{r_{ij}} \tag{9}$$

where q_i and q_j is the partial charge on atom i and j, respectively.

Table 1: Parameters [5], [33], [34] Used in UA Force Field for PDMS

E_b	d_{ij}^{o} (Å)	k_b (kcal/mol- Å^2)
Si-O	1.640	350.12
Si-CH_3	1.900	189.65
CH_2-CH_2	1.540	268.00
CH_2-N	1.448	382.00
N-H	1.010	434.00
E_θ	θ_o (deg)	k_θ (kcal/mol- rad^2)
Si-O-Si	146.46	14.14
O-Si-O	107.82	94.50
CH_3-Si-CH_3	109.24	49.97
O-Si-CH_3	110.69	49.97
CH_2-CH_2-CH_2	114.00	62.09
N-CH_2-CH_2	109.50	56.23
H-N-H	106.40	43.62

H-N- CH_2	112.90		62.09
E_θ	θ_o (deg)	k_θ^I (kcal/mol-rad^2)	k_θ^{II} (kcal/mol-rad^2)	k_θ^{III} (kcal/mol-rad^2)
Si-CH_2-CH_2	112.67	39.52	-7.44	0.00

E_ϕ	c_1(kcal/mol)	c_2 (kcal/mol)	c_3 (kcal/mol)
Si-O-Si-O	0.2250	0.0000	0.0000
Si-O-Si-CH_3	0.0000	0.0000	0.0100
O-Si-CH_2-CH_2	0.3527	-0.0677	0.7862
CH_2-CH_2-Si-CH_3	0.3527	-0.0677	0.7862
Si-CH_2-CH_2-CH_2	0.7054	-0.1355	1.5724
CH_2-CH_2-CH_2-N	1.196	-0.337	0.275
H-N- CH_2-CH_2	-0.095	-0.2085	0.209

E_{vdw}	σ_{ij}(Å)	ε_{ii}(kcal/mol)
Si-Si	4.29	0.131
O-O	3.3	0.08
CH_3-CH_3	3.75	0.1947
CH_2-CH_2	3.95	0.0914
N-N	3.34	0.2206
H-H	0.0	0.0
Si-O	3.94	0.0772
CH_3-CH_2	3.85	0.1377
Si-CH_3	3.83	0.1596
Si-CH_2	3.93	0.1093
O-CH_3	3.38	0.1247
O-CH_2	3.48	0.0854

E_{coul}	q
Si	0.387
O	-0.388
CH_3	0

For PI-PDMS copolymer, the hybrid/UA model was also used for PDMS segment, and the TraPPE-UA [35] force field was employed for the PI segment. The harmonic bond stretching and harmonic angle bending potentials given in Eq. (1) and (2) were employed. Three different torsion functional forms (Eq. (4), (10), and (11)) were used, depends on the atom types.

$$E_\phi = e_0\left[1-\cos\left(2\phi+e_1\right)\right] \tag{10}$$

$$E_{\phi} = k_{\phi}\left[1 + \cos(n\phi)\right] \tag{11}$$

In Eq. (10) and (11), e_0, e_1, and n are the constants. The nonbonded interactions terms used for PI-PDMS copolymer were similar to the nonbonded interactions used for PDMS. All parameters used for PDMS and PI are given in Table 1 and 2, respectively.

Table 2: Parameters [35], [36], [37], [38], [39], used in UA Force Field for PI

E_b	b_o (Å)	k_b (kcal/mol- Å^2)
CH_x(aro)-CH_y(aro)	1.40	469
CH_x= CH_y	1.33	481
CH_x(aro)= CH_y (aro)		
C(aro)-N(aro)	1.40	469
CH_x - CH_y	1.54	268
C-F	1.33	340
C(aro)=O	1.229	382
C-N or CH_2-N	1.448	382

E_θ	θ_o (deg)	k_θ (kcal/mol- rad^2)
CH_x(aro)-CH_y(aro)-CH_z(aro)	120.0	63.00
CH_x(aro)-N(aro)-CH_y(aro)	110.0	51.80
F-C-F	109.5	76.96
CH_x(aro)-CH_y(aro)=O	121.4	62.09
N(aro)-CH_x(aro)=O	122.9	79.99
CH_x(aro)-CH_y(aro)-CH_z	120.0	63.00
CH_x-C-CH_y	119.7	69.96
C(aro)-C(aro)-N(aro)	107.6	50.00
C-C-F	109.5	49.97
CH_2-CH_2-N(aro)	109.5	56.23

E_ϕ	c_1(kcal/mol)	c_2 (kcal/mol)	c_3 (kcal/mol)
C(aro)-C-C-F	0.15	0.0	0.20
CH_x-CH_2-CH_2-CH_y	0.3527	-0.06775	0.7862

E_ϕ	k_ϕ (kcal/mol)	n
C(aro)-N(aro)-CH_2-CH_2	0.2603	2

E_ϕ	e_o (kcal/mol)	e_1 (rad)
CH_x(aro)-C(aro)-C-C	0.33183	5π/3

E_{vdw}	σ_{ij}(Å)	ε_{ii}(kcal/mol)
CH(aro)-CH(aro)	3.695	0.10034

Caro(link)-Caro(link)	3.70	0.05961
Caro-Caro	3.88	0.04173
$C(CF_3)$-$C(CF_3)$	3.55	0.07153
C(C=O)-C(C=O)	3.72	0.06756
C(methyl)-C(methyl)	3.30	0.00795
N(aro)-N(aro)	3.45	0.05564
O(C=O)-O(C=O)	3.05	0.15697
F-F	2.95	0.04828

E_{coul}	q
CH(aro)	0
Caro	0
$C(CF_3)$	0.27
C(C=O)	0.424
C(methyl)	0
N(aro)	0
N(amine)	-0.892
O(C=O)	-0.424
F	-0.09

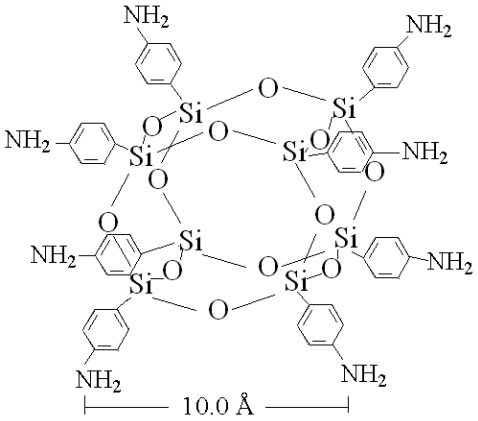

Figure 2: Structures of simulated Octaaminophenyl silsesquioxanes

The Hybrid-COMPASS (HC) force field [18], [42] was used to model the atomic interactions in OAPS. This force field includes bond stretching (E_b), angle bending (E_θ), and torsion (E_ϕ) terms which are described by equation (12), (13), and (14), respectively.

$$E_b = k_2(b - b_o)^2 + k_3(b - b_o)^3 + k_4(b - b_o)^4 \quad (12)$$

$$E_\theta = H_2(\theta - \theta_o)^2 + H_3(\theta - \theta_o)^3 + H_4(\theta - \theta_o)^4 \quad (13)$$

$$E_\phi = V_1(1 - \cos(\phi)) + V_2(1 - \cos(2\phi)) + V_3(1 - \cos(3\phi)) \quad (14)$$

where b_o is the equilibrium bond length, θ_o is the equilibrium bond angle, b is the actual bond length, θ is the actual angle, ϕ is the actual value of the dihedral angle, k_2, k_3, k_4, H_2, H_3, H_4, V_1, V_2, and V_3 are constants. The Lennard Jones (LJ) 9-6 function (E_{vdw}) was used to model the van der Waals interactions. Table 3 shows the Hybrid-COMPASS force field parameters used for this work. The nonbonded interaction terms also include the Coulombic function (E_{coul}) for electrostatic interactions. In the HC force field, the partial charge q_i is given by

$$q_i = \sum_j \delta_{ij} \tag{15}$$

where δ_{ij} is the bond increment for an atom j that is valence bonded to atom i. However, in this work, the partial charges shown in Table 4 were obtained from *ab initio* calculations done in GAMESS [40] with [6-31G(d)] [41] basis set. The mixing rules given in Eq. (7) and (8) were also employed for OAPS.

Table 3: Parameters Used in HC [18], [42] Force Field for OAPS

E_b	b_o *(Å)*	k_2 *(kcal/mol- Å^2)*	k_3 *(kcal/mol- Å^3)*	k_4 *(kcal/mol- Å^4)*
Si-C	1.899	189.65	-279.42	307.51
Si-O	1.640	359.123	-517.342	673.707
Si-H	1.478	202.78	-305.36	280.27
C_{ar}-C_{ar}	1.417	470.836	-627.618	1327.635
C-H	1.0982	372.825	-803.453	894.317
C-N	1.400	350.0	0.0	0.0
N-H	1.031	540.112	-1500.295	2431.008
E_θ	θ_o (deg)	H_2 (kcal/mol- rad^2)	H_3 (kcal/mol- rad^3)	H_4 (kcal/mol- rad^4)
C-Si-O	114.9	23.0218	-31.3993	24.9814
O-Si-O	110.7	70.3069	-6.9375	0.0
Si-O-Si	159.0	8.500	-13.4188	-4.1785
H-Si-O	107.4	57.664	-10.6506	4.6274
C-C-Si	120.0	61.0	-35.0	0.0
C-C-H	117.94	35.1558	-12.4682	0.0
C-C-C	118.9	61.0226	-34.9931	0.0
C-C-N	120.0	60.0	0.0	0.0

E_ϕ	V_1(kcal/mol)	V_2 (kcal/mol)	V_3 (kcal/mol)
Si-O-Si-O	-0.225	0.0	-0.010
Si-O-Si-H	0.0	0.0	-0.010
Si-O-Si-C	0.0	0.0	-0.010
H-C-C-H	0.0	2.35	0.0
Si-C-C-H	0.0	4.5	0.0
N-C-C- H	0.0	4.5	0.0
H-N-C-C	0.0	1.0	0.0
C_{ar}-C_{ar}-C_{ar}-C_{ar}	8.3667	1.2	0.0

E_{vdw}	σ_{ij} (Å)	ε_{ii}(kcal/mol)
Si-Si	4.405	0.1980
O-O	3.3	0.0800
H-H	2.878	0.0230
C-C	3.915	0.0680
N-N	3.83	0.0960
CH_3-CH_2	3.85	0.1377
Si-CH_3	3.83	0.1596
Si-CH_2	3.93	0.1093
O-CH_3	3.38	0.1247
O-CH_2	3.48	0.0854

Table 4: Partial Charges for atoms in the OAPS

			H(-C)	H(-N)			
Molecule	q_{Si}	q_O	q_H	q_H	q_N	q_C	
OAPS	0.876	-0.538	0.174	0.258	-0.544	C(-SiC-)	-0.204
						C(-CH-)	-0.165
						C(-CN-)	0.1043

The LJ 6-12 potential and the electrostatic potential shown in Eq. (5) and (9), respectively are also used to model the interactions between PDMS atoms and OAPS atoms; between PDMS atoms and PI atoms, and between PI atoms and OAPS atoms. The Lorentz-Berthelot [32] combining rules were also employed between these atoms.

4.2.2 Molecular dynamics details

All molecular dynamics (MD) simulations were performed using the LAMMPS [43] (Large-scale Atomic/Molecular Massively Parallel Simulator) program. For all

simulation systems, the Nose/Hoover thermostat [44] and barostat [44] were used to control the temperature and pressure, respectively. The velocity Verlet integrator was used to integrate the equations of motion. A particle-particle/particle-mesh Ewald (PPPM) algorithm [45] was used for the long range Coulombic interactions.

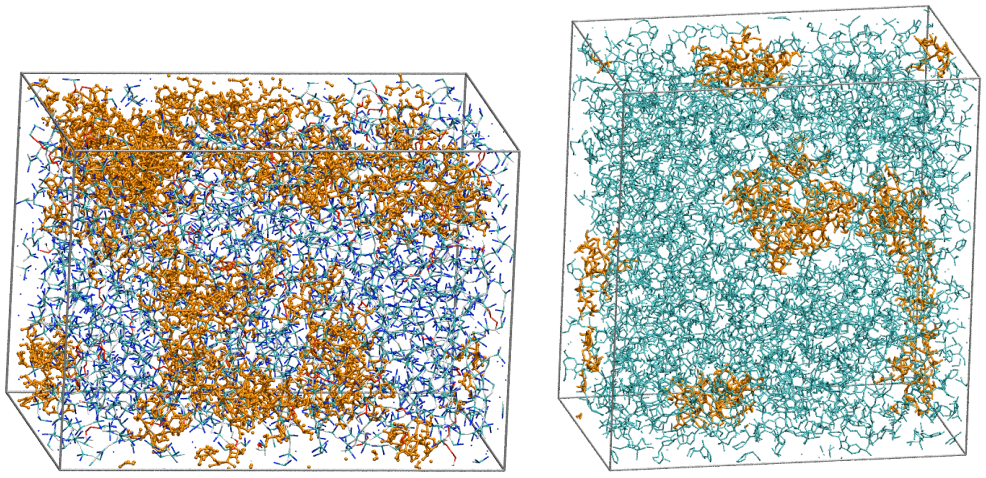

(a) (b)

Figure 3: Snapshot of equilibrated systems (orange = OAPS molecules) (a) 30.2 wt% OAPS/PDMS blends at 300K, (b) 10.96 wt% OAPS/6FDA-MDA-PDMS blends at 650K. Snapshots generated with Visual Molecular Dynamics (VMD) [46]

4.2.2.1 PDMS systems

To begin, 54 PDMS chains were placed into a simulation box at a low density. To achieve the proper density, MD simulations in NPT (constant number of particles, pressure, and temperature) ensemble were conducted at 1 atm and 600 K. The timestep used was 1 fs. Cutoff radii of 10 Å and 11 Å were used for LJ and Coulombic interactions, respectively for those systems. At 600 K, the 54 PDMS chains were relaxed for more than 5 ns. This relaxed PDMS chains was then used to start the simulation for OAPS/PDMS systems. After the addition of different weight percent of OAPS in the relaxed PDMS system, each system was again equilibrated at 600 K for 4 ns. For OAPS/PDMS blends systems, the timestep used was 0.2 fs. A number of thermodynamic

quantities were monitored; if they remained stable for more than 0.5 ns, it was concluded that the system was equilibrated. The resulting box sizes of the equilibrated configurations for all the systems are shown in Table 5.

Table 5: Equilibrated box sizes for PDMS systems at T = 600K

System	Equilibrated box sizes	Densities (g/cm^3)
54 PDMS chain	140.46 Å x 59.14 Å x 29.57 Å	0.9027
54 PDMS chain and 4.9 wt% OAPS (6 OAPS)	83.16 Å x 60.34 Å x 52.18 Å	0.8907
54 PDMS chain and 10.8 wt% OAPS (14 OAPS)	84.69 Å x 61.44 Å x 53.14 Å	0.8989
54 PDMS chain and 20.6 wt% OAPS (30 OAPS)	86.54 Å x 62.78 Å x 54.30 Å	0.9464
54 PDMS chain and 30.2 wt% OAPS (50 OAPS)	87.44 Å x 63.44 Å x 60.01 Å	0.9538

After equilibration, production runs were used to observe the properties of polymer and mixed-matrix materials, such as glass transition temperature. The glass transition temperature of a polymeric material can be determined by plotting specific volume versus temperature at constant pressure and noting where the slope changes. The specific volume as a function of temperature was obtained by performing simulations in the NPT ensemble with the temperature range of 75 K-400 K and pressure of 1 atm. The equilibrated system was cooled to lower temperatures by decreasing the temperature by an increment of 50 K for temperature higher than 200K, and an increment of 25 K for the temperature lower than 200 K. The timestep used in the production runs was 0.2 fs for temperature higher than 175 K, and 0.5 fs for the temperature equal or lower than 175 K. At each temperature, the system was run for 500 ps.

In addition to the glass transition temperatures, we have also calculated the intermolecular radial distribution functions (rdfs) for PDMS-PDMS, OAPS-OAPS, OAPS-PDMS, and the mean square displacement for OAPS and PDMS at 300K. For

these calculations, each system was run for 4.5 ns in the NPT ensemble. To ensure that the structure that we obtained in the production run is in equilibrium, we compared the rdf plots after the simulation runs of 3.5 ns, 4.0 ns, and 4.5 ns. If the difference was smaller than 5%, then the structure was concluded to be at equilibrium.

4.2.2.2 6FDA-MDA-PDMS systems

To begin, a single 6FDA-MDA-PDMS chain were placed into a simulation box at a very low density. To achieve the proper density, MD simulations in NPT (constant number of particles, pressure, and temperature) ensemble were conducted at 1 atm and 800 K. The timestep used was 1 fs for pure 6FDA-MDA-PDMS system and 0.2 fs for OAPS/6FDA-MDA-PDMS blends systems. Cutoff radii of 10 Å and 12 Å were used for LJ and Coulombic interactions, respectively. At 800 K, the single 6FDA-MDA-PDMS chain was relaxed for more than 5 ns until it formed a big coil in the simulation box. This relaxed 6FDA-MDA-PDMS chain was then used to start the simulation for each system. A number of thermodynamic quantities were monitored; if they remained stable for more than 0.5 ns, it was concluded that the system was equilibrated. The resulting box sizes of the equilibrated configurations for all the systems are shown in Table 6.

Table 6: Equilibrated box sizes for 6FDA-MDA-PDMS systems at T = 800K

System	**Equilibrated box sizes**	**Densities (g/cm^3)**
1 copolymer chain	99.71 Å x 31.91 Å x 26.14 Å	0.9357
1 chain and 4.69 wt% OAPS (2 OAPS)	42.33 Å x 44.09 Å x 40.56 Å	1.0787
1 chain and 10.96 wt% OAPS (5 OAPS)	47.37 Å x 42.29 Å x 38.91 Å	1.1210
1 chain and 19.75 wt% OAPS (10 OAPS)	48.02 Å x 42.87 Å x 39.45 Å	1.1941
1 chain and 30.7 wt% OAPS (18 OAPS)	57.14 Å x 40.82 Å x 37.55 Å	1.2822

After equilibration, production runs were used to observe the properties of copolymer and mixed-matrix materials, such as glass transition temperature. The glass transition temperature for each system was obtained by performing simulations in the

NPT ensemble with the temperature range of 300 K-800 K and pressure of 1 atm. For pure copolymer, the equilibrated system was cooled to lower temperatures by decreasing the temperature by an increment of 50 K for T higher than 700 K, and increment of 25 K for T lower than 700 K. For OAPS/6FDA-MDA-PDMS blends systems, the equilibrated system was cooled to lower temperatures by decreasing the temperature by an increment of 50 K. The process of cooling the system to the desired temperature was done with the duration of 1 ns.

The intermolecular radial distribution functions for copolymer-copolymer, OAPS-OAPS, OAPS-copolymer were also calculated at 300K. The production runs for these cases considered larger systems, which contain 4 copolymer chains. For these calculations, each system was run for about 2 ns in the NPT ensemble. To ensure an equilibrium structure, we compared the rdf plots after the simulation runs of 1 ns, 1.5 ns, and 2.0 ns. If the difference was smaller than 5%, then the structure was concluded to be at equilibrium. We also calculated mean square displacement for OAPS and PI-PDMS copolymer. However, this calculation was done at T=650 K. The production runs for this case considered large systems as well. The procedure is done by replicating twice the number of atoms in y and z directions of the equilibrated system obtained from the glass transition temperature observation. We then ran the simulation for about 1.6 ns in the NPT ensemble.

4.3 Results and Discussion

4.3.1 Glass transition temperatures

NPT molecular dynamics simulations were conducted at 1 atm to calculate the volume – temperature properties of the pure PDMS, pure PI-PDMS, OAPS/PDMS

blends, and OAPS/PI-PDMS blends. The uncertainty for the specific volume is ~ 0.01 cm^3/g, in terms of the standard error calculated for the specific volume during the production run. The specific volume versus temperature plots are shown in Figure 4 for 20.6 wt% OAPS/PDMS blends, and Figure 5 for 4.69 wt% OAPS/PI-PDMS blends. The temperature at which the slope changes represents the glass transition temperature [25], [47]. An arrow indicates the location of T_g. Simulations were also performed for the blends of 0, 4.9, 10.8, 30.2 wt% OAPS with PDMS and the blends of 0, 10.96, 19.75 wt%, 30.7 wt% OAPS with PI-PDMS copolymer. The standard error for the T_g calculation is ~ 5-10 K for PDMS systems and ~ 13-25 K for copolymer systems. These values are based on the errors associated with the two least-squares linear regression fits of the specific volume versus temperature.

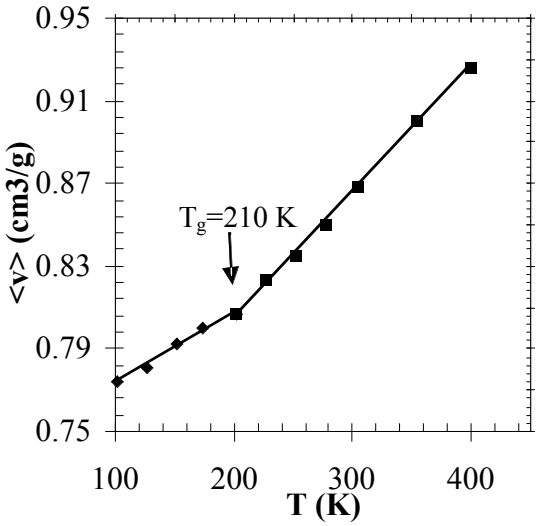

Figure 4: Specific volume vs. temperature for 20.6 wt% OAPS/PDMS blends at 1 atm obtained from NPT dynamics. The symbols indicate the state points calculated with MD simulation. The lines shown are least-squares linear regression fits through the data. The arrow indicates the position of the T_g from MD simulation.

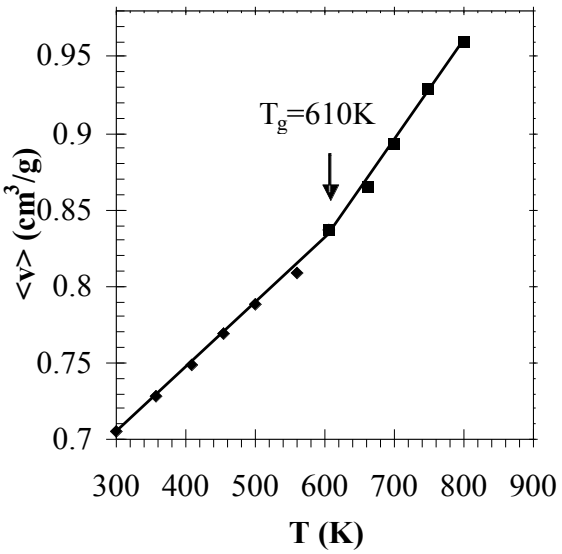

Figure 5: Specific volume vs. temperature for 4.69 wt% OAPS/PI-PDMS blends at 1 atm obtained from NPT dynamics. Symbols as in Figure 4.

Figure 6 shows a plot of T_g versus OAPS concentration for OAPS/PDMS blends systems. The simulated T_g value for pure PDMS is found to be 160 K, which is higher than the experimental value of T_g = 145 K [48]. A higher T_g value obtained from simulation is due to the limitation of the current computing resources, which is up to times of order picoseconds [49]; therefore the cooling rates are much higher (of order 10^{10} K/s). A higher cooling rate may lead to the shift of the glass transition temperature to a higher value [49], [50]. The incorporation of OAPS has caused an increase of the T_g. There is a steep increase of the T_g with the incorporation of 4.9 wt% OAPS in PDMS matrix. After that, T_g stays stable as the loading of OAPS increases up to 30.2 wt%. There are some fluctuations, which are still within the uncertainty. This trend shows that only small amount of OAPS is needed to raise the glass transition temperature of the material.

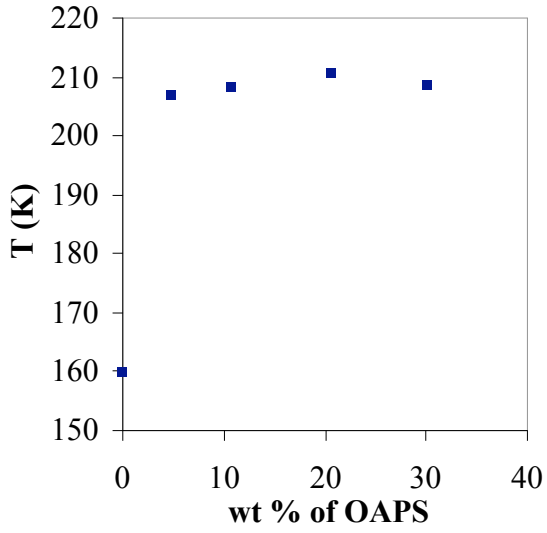

Figure 6: Effect of OAPS concentration on glass transition temperature for OAPS/PDMS blends.

Figure 7 shows a plot of T_g versus OAPS concentration for OAPS/PI-PDMS blends systems. The simulated T_g value for pure 6FDA-MDA-PDMS copolymer system is 598 K. This high T_g corresponds to the T_g for the PI phase, which is in good agreement to the T_g of the pure PI system obtained from our previous study [30]. The range of the temperature studied in this work only allowed determination of the T_g of the PI phase. Figure 7 shows that the T_g for PI phase increases as the OAPS loading increases up to 11 wt%. There is a high increase in T_g with the incorporation of 11 wt% OAPS in 6FDA-MDA-PDMS. However, with the addition of 20 wt% OAPS, the T_g value drops tremendously. This might be due to the aggregations of OAPS that have started to form for this system. After the addition of ~ 30 wt% OAPS, the T_g value continues to drop close to the T_g value at ~ 5 wt% OAPS. This observation tells us that there is no improvement of the glass transition temperature of PI-PDMS/OAPS nanocomposites with the addition of more than 11 wt% of OAPS. This result agrees with our previous

work [30] that shows no improvement of T_g for PI/OAPS nanocomposites after the addition of more than 11 wt% OAPS.

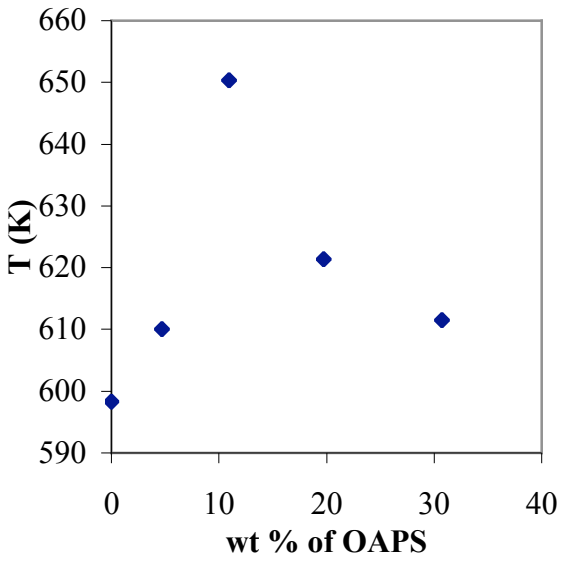

Figure 7: Effect of OAPS concentration on glass transition temperature for OAPS/6FDA-MDA-PDMS systems.

To check the effects of system size on the glass transition temperature determination, we performed two sets of simulations for the copolymer (one contains only 1 chain of copolymer, and another contains 4 chains of copolymer) to determine its glass transition temperature. Our results showed a very comparable glass transition temperature value for those two sets of simulations with uncertainty of about 2 K.

4.3.2 Radial distribution functions for PDMS Systems

The radial distribution function (rdf), g(r) provides more understanding of the POSS and polymer packing details. In this section, we present rdfs for PDMS-PDMS, OAPS-OAPS, and OAPS-PDMS. Figure 8 shows the intermolecular g(r) based on all atom centers of PDMS to PDMS in the systems. All plots show a diffuse peak at ~ 6.8 Å. This peak indicates the average interchain spacing of the PDMS chains. The presence of

OAPS did not affect the average interchain spacing of the PDMS. It is also shown that the g(r) values for PDMS with the incorporation of 4.9 and 10.8 wt% OAPS are pretty similar to the g(r) of PDMS with 0 wt% of OAPS. However, the diffuse peak of the g(r) plot for system with 20.6 wt% OAPS is slightly lower than the diffuse peak of the g(r) for pure PDMS system. The lowest g(r) values at almost all distances were found for the system with 30.2 wt% of OAPS. This indicates that the number of PDMS chain contacts in a given volume is decreased with the presence of more than 11 wt% of OAPS.

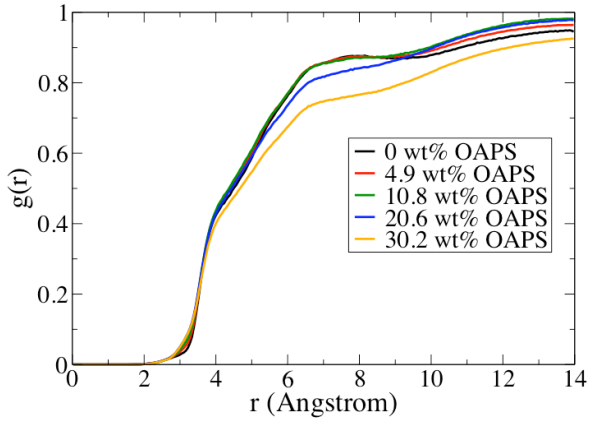

Figure 8: Radial distribution function based on all atom of PDMS to all atom of PDMS for system with different loading of OAPS at 300K.

The intermolecular packing of OAPS to OAPS based on the Si and O atoms in PDMS system is shown in Figure 9. The data from 4.9 wt% OAPS is not shown because the OAPS molecules are more dilute in the PDMS system, and therefore did not exhibit any interaction on the time scale of the simulation. The g(r) plot for 10.8 wt% OAPS system shows almost featureless OAPS coordination in the PDMS matrix. There are two diffuse peaks at ~ 11.3 Å and ~ 19.5 Å. As the OAPS loading increases, the OAPS coordination becomes more significant. This is shown by a peak found on the g(r) of 20.6 and 30.2 wt% OAPS, which is located at ~ 10.5 Å and ~ 11.3 Å, respectively. These peaks are direct evidence that there is a specific organization of the neighboring OAPS

molecules in PDMS system, indicating that a small amount of OAPS aggregation has occurred for these two systems. The aggregation can also be seen in the snapshot shown in Figure 3a.

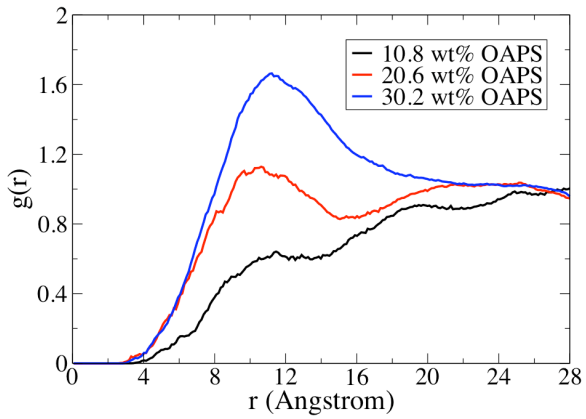

Figure 9: Radial distribution function based on POSS to POSS (Si and O atom types) for different loading of OAPS at 300K.

Figure 10 shows the intermolecular packing of the PDMS polymer chains around the OAPS at 300K. The rdf shown is based on all atom OAPS to all atom PDMS chain. All plots exhibit a diffuse peak at ~ 6.5 Å. There is no significant difference of the number density of PDMS-OAPS contacts for systems with 4.9, 10.8, and 20.6 wt% OAPS. Experimental studies have shown when the contacts between POSS and a polymer chain increases, the T_g value of the material will increase [20], [51], [52], [53]. The nearly constant T_g found for these three systems support the observation shown in Figure 10. However, the g(r) plot shows a significantly lower density of PDMS-OAPS contacts occurs for the system with 30.2 wt% OAPS, compared to the other systems. Fig. 9 has shown the most amount of OAPS aggregation for this system, on the other hand Fig. 8 has shown the least number of PDMS chain contacts. Although aggregations of

OAPS have occurred in this case, these aggregates were still able to decrease the number of PDMS chain contacts, and therefore the T_g value still stays constant.

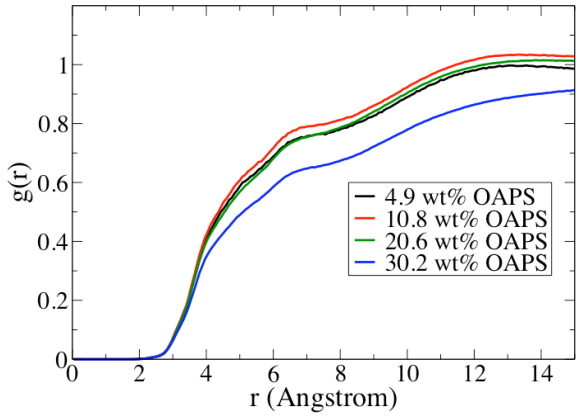

Figure 10: Radial distribution function based on all-atom POSS to all-atom PDMS for system with different wt% OAPS at 300K.

4.3.3 Radial distribution functions for 6FDA-MDA-PDMS systems

The intermolecular g(r) based on all atom centers of the 6FDA-MDA-PDMS to 6FDA-MDA-PDMS is shown in Fig. 11. All plots show a diffuse peak at ~ 6.5 Å, which indicates the average interchain spacing of the 6FDA-MDA-PDMS chains. At larger distances (10.0-12.0 Å), a very diffuse peak can be seen for all systems. The incorporation of OAPS decreased the number of contacts between 6FDA-MDA-PDMS copolymer chains. This indicates that the addition of OAPS has caused the copolymer chains to be more dispersed in the system. This observation supports the glass transition temperature results, which have shown an increase of its value with the incorporation of OAPS. As the OAPS loading increases up to 10.96 wt%, the number of the 6FDA-MDA-PDMS contacts decreases. The presence of 10.96, 19.75, and 30.7 wt% of OAPS show very similar number of 6FDA-MDA-PDMS contacts at all distances. The glass transition

temperature results have shown that there is a decrease of the value after the addition of more than 10.96 wt% OAPS in to the 6FDA-MDA-PDMS matrix.

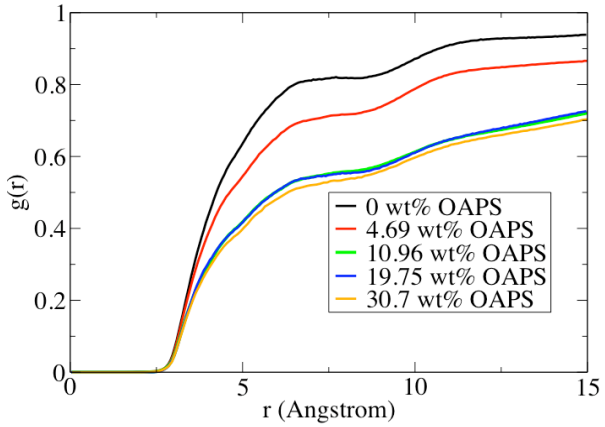

Figure 11: Radial distribution function based on all atom of 6FDA-MDA-PDMS to all atom of 6FDA-MDA-PDMS for system with different loading of OAPS at 300K.

Figure 12 shows the intermolecular packing of OAPS to OAPS based on the Si and O atoms in PI-PDMS systems. All plots indicate a liquid like structure of OAPS within the PI-PDMS system, which means a good dispersion of OAPS. There is a distinct peak shown at the distance of ~ 9.8 Å. The height of this peak decreases as the OAPS loading increases.

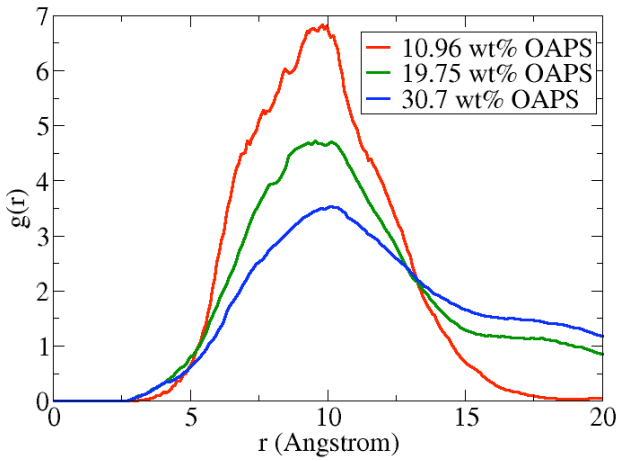

Figure 12: Radial distribution function based on all atom of OAPS to all atom of OAPS for system with different loading of OAPS at 300K.

The intermolecular structure of the 6FDA-MDA-PDMS chains around the OAPS molecules is shown in Fig. 13. There is a broad diffuse peak shown at ~ 5.0 Å for 4.69 wt% OAPS system. The diffuse peak is also shown for 10.96, 19.75, and 30.7 wt% OAPS systems, however, the peak is narrower compared to the 4.69 wt% OAPS system. The position of the peak is also shifted to a slightly smaller distance for the 10.96, 19.75, and 30.7 wt% OAPS systems. As the OAPS loading increases, the density of 6FDA-MDA-PDMS copolymer – OAPS contacts decreases.

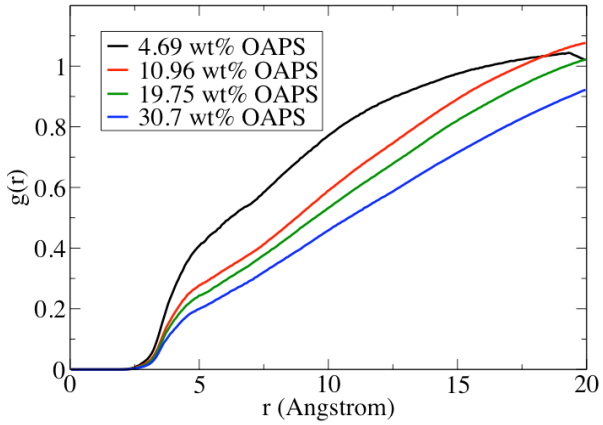

Figure 13: Radial distribution function based on all atom of OAPS to all atom of 6FDA-MDA-PDMS for system with different loading of OAPS at 300K.

The calculations of the rdfs for PI-PDMS/OAPS systems shown in Figures 11, 12, and 13 did not give much understanding of the T_g for the systems. However, there is another aspect that may cause the glass transition temperature to increase, which is with the incorporation of the relatively rigid POSS molecules, it will retard the motion of the polymer [20], [51], [54]. In the following section, the effect of POSS on the mobility of the PDMS and PI-PDMS chains will be discussed.

4.3.4 Mean square displacement for PDMS systems

To observe the mobility of PDMS and POSS in the nanocomposite materials, the mean-square displacements (MSD) for PDMS and OAPS were calculated. Figure 14

shows the MSD for PDMS chains. The MSDs for PDMS were calculated based on the chain's center of mass and averaged over the 54 chains. The incorporation of OAPS has a significant effect on the motion of PDMS chains. The PDMS moved a lot slower after the addition of OAPS. The MSD plots of PDMS chains for systems with 4.9, 10.8, 20.6, and 30.2 wt% OAPS are very similar. This indicates that there is no significant difference of the average movement of PDMS polymer chains between those systems.

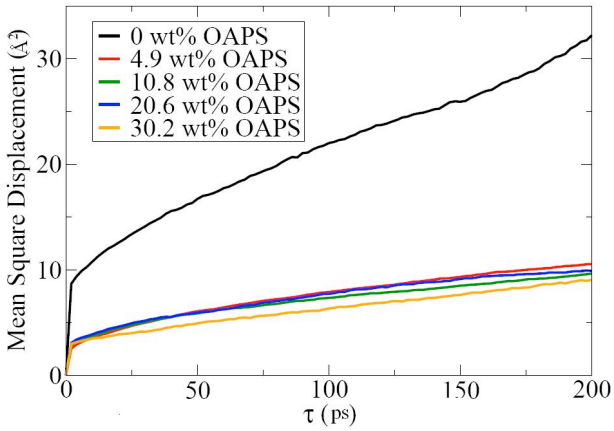

Figure 14: Mean square displacement of PDMS chains for system with different wt% OAPS at 300K.

The results from the glass transition temperature for PDMS systems have shown a tremendous increase of T_g value after the incorporation of 4.9 wt% OAPS. The significant decreased of the movement of PDMS chains have caused the material to have higher glass transition temperature. However, as seen in Figure 6, after 4.9 wt% OAPS, the T_g values stay nearly constant. This observation supports the slight difference of the MSD plots shown in Figure 14 for systems with OAPS. This means that only small amount of OAPS needed to slow down the movement of PDMS chains.

Figure 15 shows the mean square displacement of OAPS in PDMS system with different wt% of OAPS. The MSDs were calculated based on the center of mass of OAPS and averaged over all OAPS molecules in every system. The highest MSD was shown for

4.9 wt% OAPS system, which indicates OAPS molecules have higher mobility for this system. There is not much difference of the MSD values for 10.8, 20.6, and 30.2 wt% systems, which means that OAPS molecules have about the same amount of movements for these three systems.

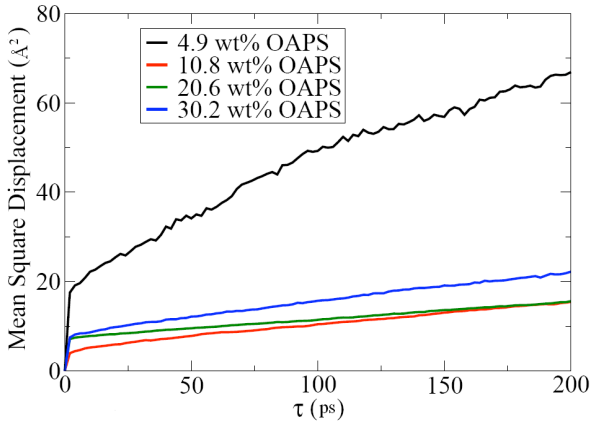

Figure 15: Mean square displacement of the POSS molecules for PDMS system with different wt% OAPS at 300K.

4.3.5 Mean square displacement for 6FDA-MDA-PDMS systems

The MSD of 6FDA-MDA-PDMS chains for all systems is shown in Fig. 16. The MSDs were calculated at a temperature above the glass transition temperature, 650K. These calculations were done based on the chain's center of mass and averaged over the 4 chains.

The mobility of PI-PDMS copolymer chain decreased with the incorporation of OAPS. These observations agree with the glass transition temperature results, which showed an increase of the T_g after the incorporation of OAPS. As the wt% of OAPS increases up to 10.96, the mobility of the copolymer decreases. The mobility of the copolymer was the slowest for system with 10.96 wt% OAPS. This observation again supports the T_g results that showed the highest T_g for this system. The MSD for 19.75 wt% OAPS is slightly higher than the MSD for 10.96 wt% OAPS. On the other hand, the

MSD of the chains for 30.7 wt% OAPS system is quite similar to the MSD of the chains for 4.69 wt% OAPS system. The T_g for these two systems also showed a very similar value.

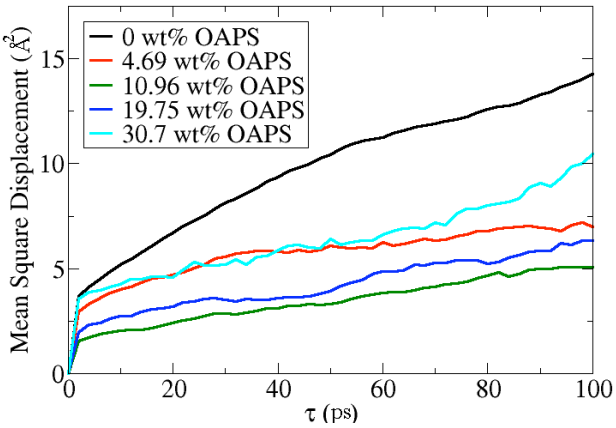

Figure 16: Mean square displacement of 6FDA-MDA-PDMS chains for system with different wt% OAPS at 650K.

Figure 17 shows the MSD plot for OAPS molecules in the PI-PDMS copolymer chains at T=650K. The MSD calculations are averaged over all OAPS molecules in each system. The mobility of OAPS decreases as the OAPS loading increases.

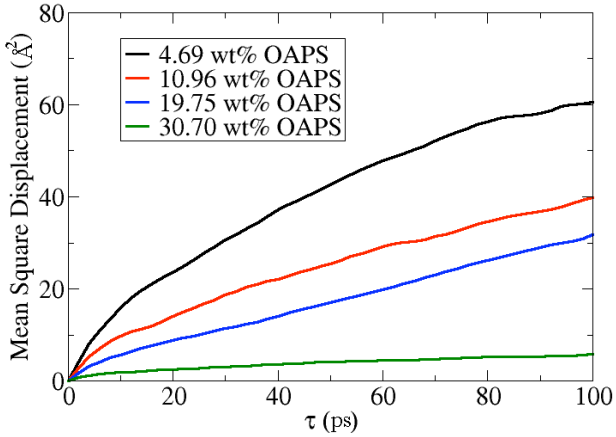

Figure 17: Mean square displacement of the POSS molecules for 6FDA-MDA-PDMS system with different wt% OAPS at 650K.

4.4 Conclusions

The effect of incorporating OAPS to PDMS polymer and to 6FDA-MDA-PDMS copolymer has been presented with atomistic molecular dynamics simulations. The

blending of OAPS into both polymer matrices showed an increase of the glass transition temperatures. The flexibility of PDMS allows more loading of OAPS, however, only small amount of OAPS is needed to raise the glass transition temperature of the material. The T_g stays nearly constant after the addition of more than 4.9 wt% OAPS. The highest T_g found for PI-PDMS/OAPS system was at about 11 wt% OAPS loading.

The mobility of PDMS, PI-PDMS chains and OAPS molecules was observed by the mean squared displacements. The incorporation of OAPS has reduced the mobility of both PDMS and PI-PDMS polymer chains. The coordination structure of OAPS and PI-PDMS do not affect much of the glass transition temperature for PI-PDMS/OAPS nanocomposites. However, the mobility of PI-PDMS copolymer chains in PI-PDMS/OAPS blends has an important role in the trend of the glass transition temperature obtained.

Acknowledgments

This work was supported by the Department of Chemical and Biological Engineering at Iowa State University. The computational work was performed at the ISU High Performance Computing facility.

References

[1] Bein T. *Chem Mat.* **1996**, 8:1636-1653.
[2] Li Y, Chung TS, Cao C, Kulprathipanja S. *J Membr Sci* **2005**, 260:45-55.
[3] Giannelis EP. *Adv Mater* (Weinheim, Ger.) **1996**, 8:29.
[4] Tsagaropolous G, Eisenberg A. *Macromolecules* **1995**, 28:6067.
[5] Striolo A, McCabe C, Cummings PT. *J Chem Phys* **2006**, 125:104904.
[6] Suer MG, Bac N, Yilmaz L. *J Memb. Sci* **1994**, 91:77-86.
[7] Li Y, Chung TS, Cao C, Kulprathipanja S. *J Membr Sci* **2005**, 260:45-55.
[8] Te Hennepe HJC, Bargeman D, Mulder MHV, Smolders CA. *J Membr Sci* **1987**, 35:39-55.
[9] Jia M, Peinemann KV, Behling RD. *J Membr Sci* **1991**, 57:289-292.
[10] Duval JM, Folkers B, Mulder MHV, Desgrandchamps G, Smolders CA. *J Membr Sci* **1993**, 80:189-198.
[11] Koros WJ, Mahajan R. *Ind Eng Chem Res* **2000**, 39:2692-2696.

12 Pechar TW, Kim S, Vaughan B, Marand E, Baranauskas V, Riffle J, Jeong HK, Tsapatsis M. *J Membr Sci* **2006**, 277:210-218.
[13] Dodiuk H, Rios PF, Dotan A, Keniq S. *Pol Adv Tech* 2007, 18: 746-750.
[14] Oaten M, Choudhury NR. *Macromolecules* 2005, 38: 6392-6401.
[15] Devaux E, Rochery M, Bourbiqot S. *Fire and Materials* 2002, 26: 149-154.
[16] Laine RM. *J Mater Chem* 2005, 15: 3725.
[17] Peng Y, McCabe C. *Mol Phys* 2007, 105: 261.
[18] Ionescu TC, Qi F, McCabe C, Striolo A, Kieffer J, Cummings PT. *J Phys Chem B* 2006, 110: 2502.
[19] Pielichowski K, Njuguna J, Janowski B, Pielichowski J. *Adv Polym Sci* 2006, 201: 225-296.
[20] Iyer P, Coleman MR. *J Appl Pol Sci* 2008, Vol. 108: 2691-2699.
[21] Lichtenhan, J. D. *Comm. Inorg. Chem.* **1995**, 17, 115-130.
[22] Mark, J. E. *Macromol. Symp.* **2003**, 201, 77-83.
[23] Li, GZ.; Wang, LC.; Ni, HL.; Pittman Jr., C. U. *J. Inorg. Organomet. Pol.* **2001**, 11, 123-154.
[24] Schwab JJ, Lichtenhan JD. *Appl. Organometal. Chem.* **1998**, 12, 707-713.
[25] Bharadwaj, R. K.; Berry, R. J.; Farmer, B. L. *Polymer* **2000**, 41, 7209.
[26] Xu, H.; Kuo, JW.; Lee, JS.; Chang, FC. *Macromolecules* **2002**, 35, 8788-8793.
[27] Striolo A, McCabe C, Cummings PT. *J Phys Chem B* 2005, 109: 14300.
[28] Fu, B. X.; Hsiao, B. S.; Pagoda, S.; Stephens, P.; White, H.; Rafailovich, M.; Sokolov, J.; Mather, P. T.; Jeon, H. G.; Phillips, S.; Lichtenhan, J.; Schwab, J. *Polymer* **2001**, 42, 599.
[29] Zheng, L.; Farris, R. J.; Coughlin, E. B. *Macromolecules* **2001**, 34, 8034-8039.
[30] Yani Y, Lamm MH. *Polymer* **2009**, 50, 1324-1332.
[31] Sun H. *Macromolecules* **1995**, 28:701.
[32]Allen MP, and Tildesley DJ. *Computer Simulation of Liquids* (Clarendon, Oxford, 1987).

[33] Frischknecht AL, Curro JG. *Macromolecules* **2003**, 36, 2122-2129.
[34] Wick CD, Stubbs JM, Rai N, Siepmann JI. *J. Phys. Chem. B* **2005**, 109, 18974-18982.
[35] Martin MG, Siepmann JI. *J. Phys. Chem. B* **1998**, 102, 2569-2577.
[36] Wick CD, Martin MG, Siepmann JI. *J. Phys. Chem. B* **2000**, 104, 8008-8016.
[37] Zhang, L.; Siepmann JI. *J. Phys. Chem. B* **2005**, 109, 2911-2919.
[38] Rai N, Siepmann JI. *J. Phys. Chem. B* **2007**, 111, 10790-10799.
[39] Rizzo RC, Jorgensen WL. *J. Am. Chem. Soc.* **1999**, 121, 4827-4836.
[40] Schmidt MW, Baldridge KK, Boatz JA, Jensen JH, Koseki S, Matsunaga N, Gordon MS, Ngugen KA, Su S, Windus TL, Elbert ST, Montgomery J, Dupuis M. *J Comput Chem* 1993, 14: 1347.
[41] (a)Hehre WJ, Ditchfield R, Pople JA. *J Phys Chem* 1972, 56: 2257. (b)Francl MM, Pietro WJ, Hehre WJ, Binkley JS, Gordon MS, Defrees DJ, Pople JA. *J Chem Phys* 1982, 77: 3654. (c)Clark T, Chandrasekhar J, Spitznagel GW, Schleyer PVR. *J Comput Chem* 1983, 4: 294. (d)Frisch, M. J.; Pople, J. A.; Binkley, J. S. *J Chem Phys* 1984, 80: 3265. (e)Okuno, Y. *J Chem Phys* 1996, 105: 5817.
[42] Sun H. *J. Phys. Chem. B* **1998**, 102, 7338-7364.

[43] Plimpton SJ. *J Comp Phys*1995, 117: 1-19.
[44] Frenkel D, Smit B. *Understanding Molecular Simulation* 2002, 2nd ed.
[45] Hockney R, Eastwood J. *Computer Simulations Using Particle*, Adam Hilger: New York, 1988.
[46] Humphrey W, Dalke A, and Schulten K. "VMD-Visual Molecular Dynamics", *J Molec Graphics*, 1996, vol. 14, pp. 33-38.
[47] Nicholson, J. W. *The Chemistry of Polymers* **2006**, 3rd Ed.
[48] Brandrup J, Immergut EH. *Polymer Handbook*, Wiley Interscience, New York, 1975.
[49] Soldera A, Grohens Y. *Macromolecules* **2001**, 35 (3), 722-726.
[50] Bizet S, Galy J, Gerard JF. *Polymer* **2006**, 47:8219-8227.
[51] Huang JC, He CB, Xiao Y, Mya KY, Dai J, Siow YP. *Polymer* 2003, 44: 4491-4499.
[52] Wahab MA, Kim I, Ha CS. *Polymer* 2003, 44: 4705.
[53] Xiong M, You B, Shuxue Z, Limin W. *Polymer* 2004, 45: 2967.
[54] Lee A. *Mat Res Soc Symp Proc* 1999, Vol. 576: 343-350.

CHAPTER 5 COARSE-GRAINED MODEL FOR OCTAHYDRIDO SILSESQUIOXANE

Abstract

The force-matching approach is presented for obtaining a coarse-grained (CG) force field for octahydrido silsesquioxane (OHS) from a molecular dynamics (MD) simulation with the atomistic effective fragment potential (EFP). The method was applied to derive a one-site pairwise force field for the OHS molecule. Two different system sizes of the atomistic MD simulations were used. The structural properties of OHS were observed to validate the CG model by calculating the radial distribution function based on the center of mass. The CG model is found to be able to reproduce the structural properties of OHS from the atomistic MD simulation.

5.1 Introduction

Polyhedral oligomeric silsesquioxane (POSS) is a cage structure consisting of silicon and oxygen atoms. It has a chemical composition of $(RSiO_{1.5})_n$ (n = 4, 6, 8, 10…) with R as an organic functional group. The most commonly studied POSS molecule is the octasilsesquioxane, $(RSiO_{1.5})_8$, which has a cube-shaped Si_8O_{12} cage with organic groups R at each corner [1]. POSS was first studied experimentally to predict its crystal structure [2], [3], [4]. Auf der Heyde *et al*. [5] has obtained the starting unit cell fractional coordinates for $H_8Si_8O_{12}$ with a density of 1.97 g/cm^3 at T=100K. They found out that the crystal structure arrangement is hexagonal and the unit cell contains three molecules [5].

It has been pointed out in the literature that the functional groups present on POSS influence its important physical properties such as melting point and crystal structure.

Thus, in order to determine these properties, many synthetic methods have been developed to explore the modifications of the selective organics groups on POSS [6], [7].

POSS can potentially be incorporated in a polymer to form a nanocomposite material. This can be done either by physically blending the POSS molecules with the polymer or by chemically introducing them as pendant groups on the polymer backbone [8], [9], [10]. The incorporation of POSS molecules into polymer results in the improvement of material properties such as increase in thermal stability, increase in glass transition temperatures, heat resistance, reductions in flammability and heat evolution [1], [8], [9]. The effect of POSS on polymeric materials has been studied in simulation works [1], [8], [9], [10] as well as in experimental works [11], [12].

Whether the POSS molecules are uniformly dispersed within the polymer or aggregate to form clusters [10], [12], such observations are critical in nanocomposite materials. In the last decade, atomistic molecular simulations have contributed to our knowledge about the fundamental interactions between polymer and POSS species. However, there is a limitation of the system size and the time scale to study such macromolecular system in an atomistic simulation. The computational limitations restrict the atomistic simulation to the timescales on the order of picoseconds [13].

The typical time scale for most interesting phenomena occurring in a macromolecular system, such as, self-assembly of polymers [14], protein folding [15], can range from nanoseconds to microseconds. Therefore, in order to further simplify the atomistic model, there is an alternative approach, called a coarse-grained (CG) model that has been used for modeling macromolecular systems. A CG model eliminates the unimportant degrees of freedom in the simulation by treating a collection of atoms as one

coarse-grained site, and therefore, larger systems can be considered at longer time scales. This scheme can be seen in Figure 1. The coarse-grained site is usually the center of mass or geometric center of the atom groups. Then, the effective interaction potentials between the coarse-grained sites are determined. These potentials are then used in the CG simulation to obtain properties, which are comparable to the atomistic simulation.

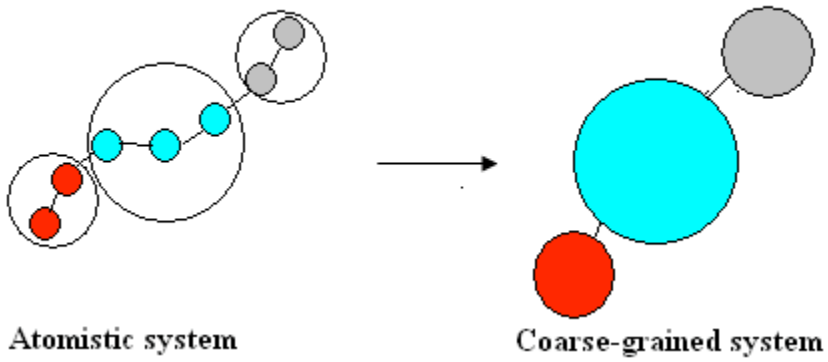

Figure 1: Coarse-graining scheme

Some approaches to obtain the potentials by coarse-graining include optimizing the parameters by: fitting it to the desired property [16], [17], [18]; structure matching [19], [20]; or force matching (FM) [21], [22]. Chan *et al*. [20] have developed a CG model using a structural-based scheme to simulate self-assembly for nonyl-tethered POSS molecules dissolved in hexane solvent. Their results showed a small aggregate of POSS molecules, which is similar to the one obtained with atomistic simulations. They also reported that their CG model reduced computational time by about two orders of magnitude compared to simulations with the equivalent atomistic model.

This work will focus on the force-matching method. The force-matching method can determine a pairwise force field from a given trajectory and force data from *ab initio* simulation or any classical atomistic molecular simulation. This method was first

introduced by Ercolessi and Adams [21]. They determined a method for least-squares fitting of the potential to the force data calculated from *ab initio* calculation [21]. Their force-matching method was mainly applied to elemental systems, such as metals.

Izvekov *et al*. [22] then developed a new force-matching method that can only parametrize the classical force field if it is linearly dependent on the fitting parameters. This can usually be achieved through spline interpolations. The Voth group has successfully employed this method to obtain the CG model of dimyristoylphosphatidylcholine (DPMS) lipid bilayer [23]. Their CG model was able to reproduce the structural properties of a lipid bilayer from the atomistic simulation. It was also stated that their approach was computationally not expensive. The gain in speed of their CG simulation compared to the atomistic simulation was about 50 times. The force-matching method has also been successfully employed to obtain the CG model of condensed-phase systems [22], [24]; ionic liquids [25], [26], and also C_{60} and carbonaceous nanoparticles [27].

In the current work, a one-site coarse-grained model for octahydrido silsesquioxanes (OHS) ($H_8Si_8O_{12}$) is derived from the trajectory and force data obtained from effective fragment potential (EFP) molecular dynamics (MD) simulation. EFP was developed by Day, *et al*. [28]. It is not only capable of modeling solvent effects [28], [29], but also can be used to study clusters of solvent molecules [30], [31]. Day, *et al*. [31] successfully applied the potential from EFP method to accurately simulate the intermolecular interactions for water clusters. They utilized the polarized double-zeta basis set of Dunning and Hay [32] [DH(*d,p*)]. From their work, it was shown that EFP method can accurately reproduce bulk or cluster properties for water.

The paper is organized as follows: in Section 2, a detailed explanation of the EFP, force-matching method are provided and the molecular dynamics simulation method is explained; in Section 3, the validation of the CG model of OHS is discussed; and in Section 4, a summary of the findings is provided.

5.2 Methods

5.2.1 Effective Fragment Potential (EFP)

The EFP parameters for an optimized geometry of $H_8Si_8O_{12}$ were obtained from the *ab initio* calculation using GAMESS [33] (general atomic and molecular electronic structure system) program. The T_8 POSS ($H_8Si_8O_{12}$) molecule was optimized by Kudo *et al.* [34] using B3LYP hybrid density functional theory [35] with [6-31G(d)] [36] basis set. In the current work, the basis set used to obtain the EFP parameters was [6-311G**] [37].

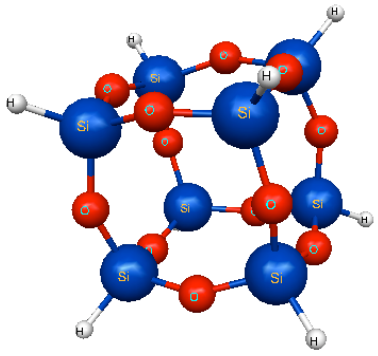

Figure 2: Optimized structure of octahydrido silsesquioxane

The EFP model uses a rigid body approximation, which means that the internal coordinates for each POSS molecule fragment are fixed (Si-O bond = 1.624Å, Si-H bond = 1.455Å, O-Si-O angle = 108.41°, O-Si-H angle = 110.51°). The EFP model developed in GAMESS is based on several quantum mechanics methods [38]. It treats molecules as

one electron effects. The types of interactions included in the effective fragment potential are shown in Eq. (1):

$$E_{\text{int}eraction} = E_{coul.} + E_{pol.} + E_{\text{Re}m.} \quad (1)$$

where, $E_{coul.}$ is the Coulomb interactions and described by a distributed multipolar expansion of fragment charge, dipole, quadrupole, and octopole; $E_{pol.}$ is the polarization interaction energy with the polarizabilities centered on localized molecular orbitals, and $E_{Rem.}$ describes the remainder interactions that are not accounted from the previous two terms [38].

There are two types of EFP available in GAMESS: EFP1 which is used specifically for water, and EFP2, the general version of the method that can be used for any species. EFP2 is derived from first principles [38], [39], and used for the current work. For EFP2, the third term in Eq. (1) consists of the interactions due to the exchange repulsion, dispersion, and charge transfer. With the EFP parameters, MD simulations were then performed using GAMESS [33]. The simulations used a periodic boundary condition and a time step of 2.0 fs. The velocity verlet type of MD integrator was applied.

Two different systems with a density of 0.71 g/cm^3 were considered for the EFP MD simulation. First system contains 36 OHS molecules in a cubic box with a side length of 33 Å, and the second system contains 64 OHS molecules in a cubic box with a side length of 40 Å. The procedure includes equilibration and production runs, both using NVT (constant number of molecules, constant volume, and constant temperature) ensemble. All runs were performed at T = 500K. The Nose/Hoover thermostat [40] was used to control the temperature.

The system containing 36 OHS was equilibrated for 9 ps and then a production run of 25 ps was performed to obtain the trajectory and force data. The 64 OHS molecules system was also equilibrated for 9 ps before the production run of 40 ps. The trajectory and force data were sampled at an interval of 0.1 ps.

5.2.2 Force Matching Method [22], [41]

This method is done to obtain the effective pair force between the coarse grained sites. First, the CG sites of the OHS molecules were determined. A one coarse-grained site represents one POSS molecule. This scheme is shown in Figure 3. The position of the atoms and the net forces acting on the center of mass of OHS molecule obtained from EFP MD simulation are then converted to the positions and forces of the CG sites. In this case, the position of each CG site is the center of mass of OHS molecule, and the net force of one CG site is the sum of the net forces acting on all the atoms of OHS molecule. The net force of each CG site can be expressed as

$$F_i = \sum_{j=1}^{N} f_{ij} \qquad i=1, 2, 3\ldots N\ ;\ j \neq i \qquad (2)$$

where, N is the total number of CG sites (36 and 64 in this work), and f_{ij} is the pair force between CG site *i* and *j*. This pair force, f_{ij} is unknown, therefore, a model, $f_{ij}(r_{ij}, b_1, b_2, b_3 \ldots b_M)$ is chosen such that each force model will depend linearly on a set of *M* parameters.

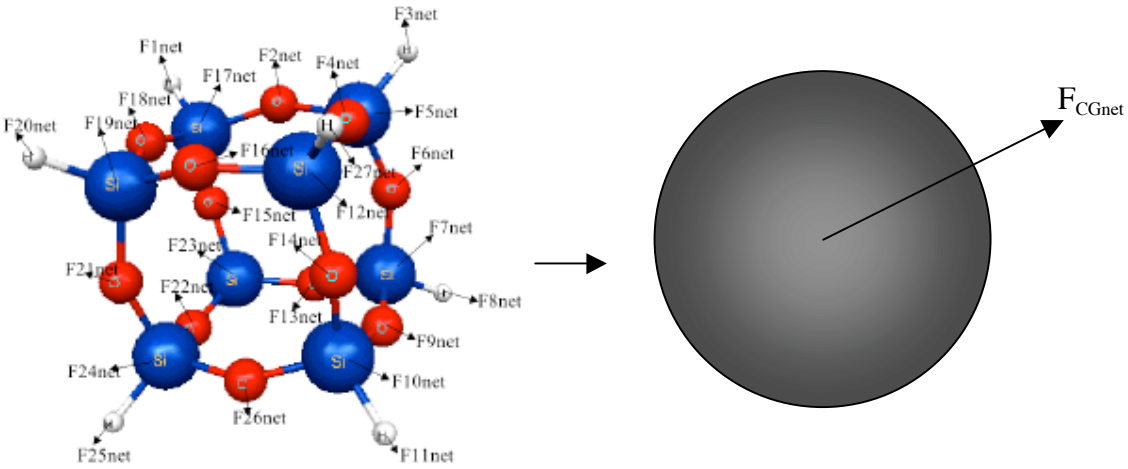

Figure 3: Coarse-graining scheme for octahydrido silsesuiqoxane

To solve for the pair force of the coarse-grained sites, a cubic spline (third order polynomials) interpolation is employed. The cubic spline interpolation has the advantages of not only having a continuous function across the mesh but also having continuous first and second derivatives. Therefore, this will ensure a smooth curvature across the mesh points.

If the distance of r_{ij} is divided into a set of mesh points $\{r_k\}$, then $f_{ij}(r_{ij})$ in the k^{th} mesh ($r_k \le r_{ij} \le r_{k+1}$) can be written as

$$f_{ij}\left(r_k \le r_{ij} \le r_{k+1}\right) = A\left(r_k, r_{ij}, r_{k+1}\right) f\big|_k + B\left(r_k, r_{ij}, r_{k+1}\right) f\big|_{k+1} + C\left(r_k, r_{ij}, r_{k+1}\right) f''\big|_k + A\left(r_k, r_{ij}, r_{k+1}\right) f''\big|_{k+1} \quad (3)$$

where A, B, C, and D are known functions of r_{ij}, r_k, and r_{k+1}, and $f''|_k$ is the second derivative of the pair-force at distance r_k.

By using the pair force expression, shown in Eq. (3), Eq. (2) with M unknowns can then be solved in a least-squares sense by using the singular value decomposition. However, to minimize the error of the pair force calculation and to get an average value of the pair force, an overdetermined system is expected, in which $N > M$. If $N < M$, more

equations of the pair force can be obtained from the MD simulation at the different timestep so that the number of equation is greater than the number of unknown.

5.2.3 Molecular dynamics details

The CG pair potentials were obtained by integrating the pair forces produced from force-matching method explained above. These potentials are used for the CG MD simulation. To validate the coarse-grained model, the radial distribution function (rdf) was calculated based on the center of mass of the CG site and compared to the rdf based on the center of mass of OHS molecules obtained from the EFP MD simulation. The CG systems considered are 36 OHS CG site and 64 OHS CG site systems with the density of 0.71 g/cm^3. The CG MD simulations were done in NVT (constant number of molecules, constant volume, and constant temperature) ensemble at 500 K. The timestep used was 5.0 fs, and each simulation was run for 15.0 ns.

In addition, the structural properties for OHS obtained from the CG MD simulation were compared to the properties obtained from another molecular mechanics force field, Hybrid COMPASS (HC) [42]. Ionescu *et al*. [1] has shown that the structural properties for OHS obtained with HC force field are in good agreement with the experimental data.

The parameters used for HC atomistic simulation were similar to the one used in our previous work [43]. For comparison, a 512 OHS molecule system and a 512 CG site system were considered for the atomistic simulation and for the CG-MD simulation, respectively. Both systems have a density of 1.52 g/cm^3. The simulation was conducted in the NVT ensemble at T = 500K. The Nose/Hoover thermostat [40] was used to control the temperature. The simulations used a periodic boundary condition. A time step of 1.0

fs and 5 fs were used for atomistic and CG simulation, respectively. The atomistic MD system was first equilibrated for 2.0 ns and then a production run of 4.0 ns was performed to obtain the radial distribution function for OHS molecules. The CG-MD simulation was equilibrated for 5.0 ns and a production run of 10.0 ns was performed to obtain the rdf based on the center of masses of the CG sites. The CG MD and HC MD simulations were performed using the LAMMPS [44] (Large-scale Atomic/Molecular Massively Parallel Simulator) program.

5.3 Results and Discussion

5.3.1 Force-Matching

Figure 4a shows the pairwise forces fitted to data from EFP MD simulation of systems of 36 and 64 OHS molecules. The plots show no significant difference between the pair forces obtained from fitting the trajectory and the force data produced from those two EFP MD simulations. The energy pair potential for these two cases is shown in Figure 4b.

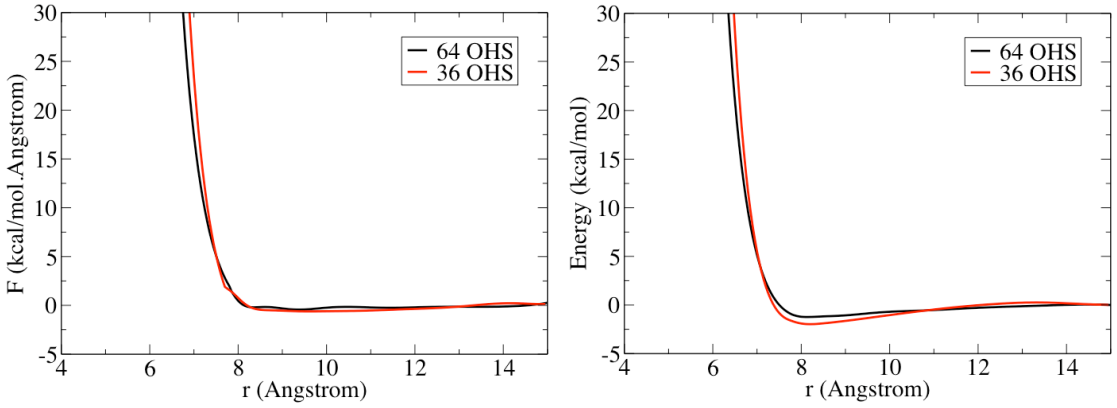

(a) (b)

Figure 4: Coarse-grained force field results obtained by fitting to the trajectory and force data produced by EFP MD simulations of systems of 36 and 64 OHS molecules: (a) Effective pairwise forces between OHS CG interaction sites as a function of intersite separation obtained from force-matching method. (b) Effective pair potential between OHS CG interaction sites as a function of intersite separation obtained by integrating the pair forces.

5.3.2 Radial distribution functions (RDF)

The RDF or g(r) is a pair correlation function that determines the probability of finding atoms at a distance *r* from a reference particle. The RDFs were calculated based on the centers of mass of OHS CG sites. Figure 5 shows that our CG model for OHS molecules were able to reproduce the same structure of OHS based on the center of masses to the structure obtained from the EFP atomistic MD simulation. The two peaks of the rdf plot were reproduced at exactly same position with the same height.

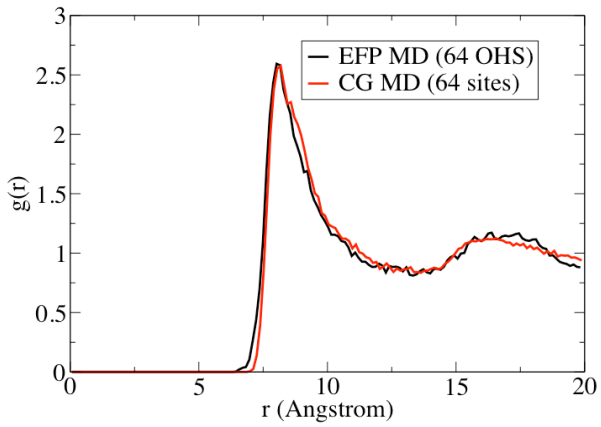

Figure 5: Radial distribution function based on the center of mass to the center of mass of OHS for system with 64 molecules (density=0.71 g/cm^3) obtained from EFP MD and CG MD simulations at 500K.

Figure 6a compares the rdf plot obtained from using CG force field produced by fitting 36 OHS molecules to the one produced by fitting 64 OHS molecules. There is a noticeable difference between the rdf plots for the two system sizes. This trend is also shown for the rdf plots obtained from the EFP atomistic simulation shown in Figure 6b.

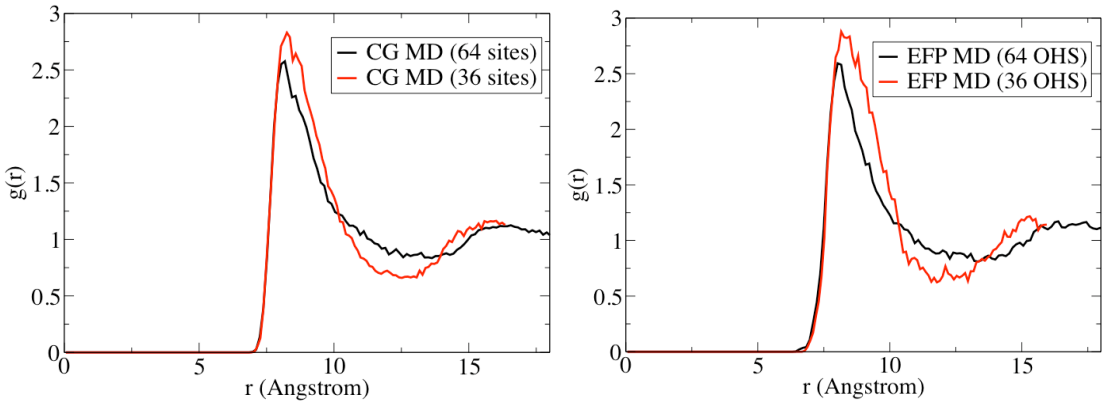

(a) (b)

Figure 6: Comparison of OHS-OHS radial distribution functions from 36 and 64 OHS molecule systems (density=0.71 g/cm^3) at 500K.

The rdf plots shown in Figure 7 suggest that our CG model was also able to reproduce a reasonably good agreement of the OHS structure to the structure obtained from HC atomistic model at the temperature of 500 K and the density of 1.52 g/cm^3. As mentioned earlier, HC force field is known to be able to reproduce the experimental structure of OHS molecules. The rdf plot from CG MD simulation was able to reproduce the peak at the distances of ~ 8 Å, 15 Å, and 22 Å. The peaks of the rdf plot obtained from CG MD simulation after the distance of 12 Å are smoother compared to the peaks obtained from the HC MD simulation. This is reasonable due to that in the atomistic model, the arrangement of OHS molecules involves all atoms (Si, O, and H), however, the arrangement of OHS molecules for CG model only involves one type of spherical particle.

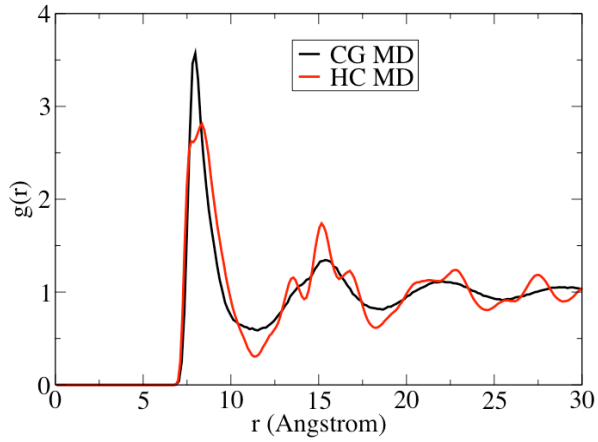

Figure 7: Radial distribution function based on the center of mass of OHS obtained with CG force field and HC force field at 500 K with the density of 1.52 g/cm^3.

5.4 Conclusions

We derived a one site coarse-grained force field for octahydrido silsesquioxane by using force-matching method. The pairwise forces were obtained by fitting to the trajectory and force data produced from EFP MD simulation of systems of 36 and 64 OHS molecules. The CG model was tested by comparing the radial distribution function obtained from the CG MD simulation to the radial distribution function obtained from the EFP MD simulation. The CG model was able to accurately reproduce the radial distribution function plot from the EFP atomistic simulation. Our CG model was also able to obtain a close agreement of the structural property of OHS to the one obtained from the Hybrid COMPASS atomistic simulation. The current CG model has provided three orders of magnitude speed up in CPU time compared to the HC atomistic model of similar systems.

References

[1] Ionescu, T. C.; Qi, F.; McCabe, C.; Striolo, A.; Kieffer, J.; Cummings, P. T. *J. Phys. Chem. B* **2006**, 110, 2502.
[2] Larsson, K. *Ark. Kemi* **1960**, 16, 203.
[3] Larsson, K. *Ark. Kemi* **1960**, 16, 209.

[4] Larsson, K. *Ark. Kemi* **1960**, 16, 215.
[5] Auf der Heyde, T. P. E.; Burgi, H. B.; Burgy, H.; Tornroos, K. W. *Chimia* **1991**, 45, 38.
[6] Voss, E. J.; Sabat, M.; Shriver, D. F. *Inorg. Chem.* **1991**, 30, 2707.
[7] Laine, R. M.; Zhang, C.; Sellinger, A.; Viculis, L. *Appl. Organometal. Chem.* **1998**, 12, 715.
[8] Peng, Y.; McCabe, C. *Mol. Phys.* **2007**, 105, 261.
[9] Bharadwaj, R. K.; Berry, R. J.; Farmer, B. L. *Polymer* **2000**, 41, 7209.
[10] Striolo, A.; McCabe, C.; Cummings, P. T. J. *Phys. Chem. B* **2005**, 109, 14300.
[11] Xu, HY.; Kuo, XW.; Lee, JS.; Chang, FC. *Macromolecules* **2002**, 35, 8788-8793.
[12] Fu, B. X.; Hsiao, B. S.; Pagola, S.; Stephens, P.; White, H., Rafailovich, M.; Sokolov, J.; Mather, P. T.; Jeon, H. G.; Phillips, S.; Lichtenhan, J.; Schwab, J. *Polymer* **2001**, 42, 599-611.
[13] Soldera A, Grohens Y. *Macromolecules* **2001**, 35 (3), 722-726.
[14] Chushak, Y; Travesset, A. *J Chem Phys* **2005**, 123, 234905.
[15]Nielsen, SO; Lopez, CF; Srinivas, G; Klein, ML. *J Phys Cond Mat* **2004**, 16, R481-R512.
[16] Shelley JC, Shelley MY, Reeder RC, Bandyopadhyay S, Klein ML. *J Phys Chem B* **2001**, 105:4464-4470.
[17] Shelley JC, Shelley MY, Reeder RC, Bandyopadhyay S, Moore PB, Klein ML. *J Phys Chem B* **2001**, 105:9785-9792.
[18] Harmandaris VA, Adhikari NP, van der Vegt NFA, Kremer K. *Macromolecules* **2006,** 39, (19), 6708-6719.
[19] McGreevy RL, Pusztai L. *Molecular Simulation* **1988,** 1, (6), 359 - 367.
[20] Chan, ER; Stiolo, A; McCabe, C; Cummings, PT; Glotzer SC. J Chem Phys **2007**, 127:114102.
[21] Ercolessi F, Adams JB. *Europhys Lett* **1994**, 26:583-588.
[22] Izvekov, S.; Parrinello, M.; Burnham, C. J.; Voth, G. A. *J. Chem. Phys.* **2004**, 120, 10896.
[23] Izvekov, S.; Voth, G. A. *J. Phys. Chem. B* **2005**, 109, 2469.
[24] Izvekov S, Voth GA. *J Phys Chem B* **2005,** 109, (14), 6573-6586.
[25] Wang YT, Izvekov S, Yan TY, Voth GA. *J Phys Chem B* **2006,** 110, (8), 3564-3575.
[26] Wang YT, Izvekov S, Yan TY, Voth GA. *J Phys Chem B* **2006,** 110, (37), 18601-18608.
[27] Izvekov S, Violi A, Voth GA. *J Phys Chem* **2005**, 109 (36), 17019-17024.
[28] Day, P. N.; Hensen, J. H.; Gordon, M. S.; Webb, S. P.; Stevens, W. J.; Krauss, M.; Garmer, D.; Basch, H.; and Cohen, D. *J. Chem. Phys.* **1996**, 105, 1968.
[29] Chen, W.; Gordon, M. S. *J. Chem. Phys.* **1996**, 105, 11081.
[30] Merrill, G. N.; Gordon, M. S. *J. Phys. Chem. A* **1998**, 102, 2650.
[31] Day, P. N.; Pachter, R.; Gordon, M. S.; Merrill, G. N. A *J. Chem. Phys.* **2000**, 112, 2063.
[32] Dunning, T. H. J.; Hay, P. J. *Methods of Electronic Structure Theory* (Plenum, New York, 1977).

[33] Schmidt, M. W.; Baldridge, K. K.; Boatz, J. A.; Jensen, J. H.; Koseki, S.; Matsunaga, N.; Gordon, M. S.; Ngugen, K. A.; Su, S.; Windus, T. L.; Elbert, S. T.; Montgomery, J.; Dupuis, M. *J. Comput. Chem.* **1993**, 14, 1347.
[34] Kudo, T.; Machida, K.; Gordon, M. S. *J. Phys. Chem. A* **2005**, 109, 5424-5429.
[35] (a)Lee, C.; Yang, W.; Parr, R. G. *Phys. Rev.* **1988**, B37, 785. (b)Miehlich, B.; Savin, A.; Stoll, H.; Preuss, H. *Chem. Phys. Let.* **1989**, 157, 200-206. (c)Becke, A. D. *J. Phys. Chem.* **1993**, 98, 5648.
[36] (a)Hehre, W. J.; Ditchfield, R.; Pople, J. A. *J. Phys. Chem.* **1972**, 56, 2257. (b)Francl, M. M.; Pietro, W. J.; Hehre, W. J.; Binkley, J. S.; Gordon, M. S.; Defrees, D. J.; Pople, J. A. *J. Chem. Phys.* **1982**, 77, 3654. (c)Clark, T.; Chandrasekhar, J.; Spitznagel, G. W.; Schleyer, P. V. R. *J. Comput. Chem.* **1983**, 4, 294. (d)Frisch, M. J.; Pople, J. A.; Binkley, J. S. *J. Chem. Phys.* **1984**, 80, 3265. (e)Okuno, Y. *J. Chem. Phys.* **1996**, 105, 5817.
[37] Krishnan, R.; Binkley, J. S.; Seeger, R.; Pople, J. A. *J. Chem. Phys.* **1980**, 72, 650.
[38] Netzloff, H. M.; Gordon, M. S. *J. Chem. Phys.* **2004**, 121, 2711.
[39] Gordon, M. S.; Freitag, M. A.; Bandyopadhyay, P.; Jensen, J. H.; Kairys, V.; Stevens, W. J. *J. Phys. Chem. A* **2001**, 105, 293-307.
[40] Frenkel D, Smit B. *Understanding Molecular Simulation* 2002, 2nd ed.
[41] Pranami G, Slipchenko L, Lamm MH, Gordon MS. *Coarse-grained intermolecular potentials derived from the effective fragment potential: Application to water, benzene, and carbon tetrachloride, chapter in Multi-Scale Quantum Models for Biocatalysis: Modern Techniques and Applications, in the Series, Challenges and Advances in Computational Chemistry and Physics*, Springer Verlag
[42] Sun H. *J. Phys. Chem. B* **1998**, 102, 7338-7364.
[43] Yani, Y; Lamm MH. *Polymer* **2009**, 50, 1324-1332.
[44] Plimpton SJ. *J Comp Phys***1995**, 117: 1-19.

CHAPTER 6 CONCLUSIONS AND FUTURE WORK

The overall objective of this work is to use a molecular dynamics simulation to analyze the thermal properties of a mixed matrix material, which will then be used to design a mixed matrix membrane for hydrogen gas separation. The incorporation of the inorganic filler within the polymer matrix is expected to increase the thermal stability of the material. In order to design such a robust membrane for this application, several things need to be considered, such as, the type of polymer and inorganic fillers used, and also percent loading of the inorganic fillers. The primary material property that we study is the glass transition temperature. The addition of the inorganic fillers may result to an increase or a decrease of the glass transition temperatures.

Three different types of polymers have been considered in this study: a glassy polymer (6FDA-MDA polyimide), a flexible polymer (poly(dimethyl siloxane)), and a combination of glassy and flexible copolymer (6FDA-MDA-PDMS). The inorganic fillers that we have considered in this work are polyhedral oligomeric silsesquioxanes (POSS). The octahydrido silsesquioxane (OHS) and the octaaminophenyl silsesquioxane (OAPS) were incorporated within the polyimide matrix. Our results showed that the addition of OHS into polyimide matrix exhibited no improvement in the thermal stability of the material. This is shown with the decrease of the glass transition temperature. On the other hand, an increase of the glass transition temperature was resulted with the incorporation of OAPS within the polyimide matrix. The optimum number of OAPS loading which has the biggest impact in improving the glass transition temperature was determined to be about 11 wt%. Our simulated glass transition temperature results have also shown a qualitative good agreement to the experimental results.

In addition, the incorporation of OAPS into PDMS matrix and 6FDA-MDA-PDMS matrix have also shown the increase of the glass transition temperatures. Only a small amount of OAPS was needed in the PDMS matrix in order to result in a significant increase in the glass transition temperature. Although the flexible nature of PDMS polymer which allows more OAPS molecules to be incorporated into the system, the glass transition temperatures were found to increase only slightly with the high loading of OAPS compared to the low loading of OAPS. In our model, the optimum number of OAPS loading for PDMS system is about 20 wt%.

The 6FDA-MDA-PDMS copolymer used in this work contains about 24 wt% of PDMS. The glass transition temperature found for the copolymer systems corresponds to the glass transition temperature for the polyimide phase. The optimum number of OAPS loading for the copolymer systems is about 11 wt%, which is similar to the optimum number of OAPS loading for polyimide systems.

It has been stated that the increase or decrease of the glass transition temperature of the mixed matrix material may be due to the polymer-inorganic filler phase behavior or the rigidity of the inorganic filler which can reduce the mobility of the polymer. To understand these behaviors, the radial distribution functions (rdfs) based on POSS to POSS, polymer to POSS, and polymer to polymer and also the mean square displacements (MSD) of POSS and polymer are calculated. The radial distribution functions provide more understanding of the POSS and polymer packing details, and the MSDs provide the understanding of the mobility of POSS and polymer. In general, our rdfs and MSD results supported the trend found in the glass transition temperature results. Our studies have also shown that the most important factor that affects the glass transition

temperature of the nanocomposite material to increase or decrease is the mobility of the polymer chains in the material.

Although the atomistic simulations study that we have done have provided a good understanding of the effect of the POSS incorporation into a polymer matrix to the thermal properties, the atomistic simulation has a limitation to the size of a system and also the time scale being used. As we know, in practical applications, it usually requires a larger system size, which means a larger simulated time scales will be needed. To overcome this situation, a further simplification of the atomistic model is necessary. Coarse-grained (CG) approaches have been known with such objective. In our last study, we have determined a coarse grained model for the octahydrido silsesquioxane (OHS) molecule by using the force-matching method. Our CG model was able to obtain a good agreement of the structural property of OHS to the atomistic model. The CG model has also provided three orders of magnitude speed up in CPU time compared to the Hybrid COMPASS atomistic simulation.

The current atomistic simulation studies for the nanocomposite materials have only considered blending POSS molecules in a polymer matrix. It would be interesting to study the nanocomposite materials by either introducing the POSS molecule as pendant groups on the polymer chain or by covalent binding it within the polymer backbone. In addition, the coarse-grained model for PI/OHS, PI/OAPS, PDMS/OAPS, and PI-PDMS/OAPS blends can also be studied in the future. With the CG model, larger system size with longer time scale can be considered for those mixed-matrix materials. By using the larger system, the transport properties, such as permeabilities, solubilities,

selectivities, and diffusivities of several gases may be obtained and compared to the experiment and then to be used in membrane applications.

ACKNOWLEDGMENTS

First and foremost, I would like to express my sincere thanks to my major professor, Dr. Monica H. Lamm for her guidance, encouragement, understanding, and advice throughout the years of my graduate study at Iowa State University.

I would also like to thank Dr. Mark S. Gordon, Dr. R. Dennis Vigil, Dr. Eric W. Cochran, and Dr. Zhiqun Lin for their useful advice and their efforts in serving on my graduate committee. Thanks to Dr. Maria Coleman, Dr. Pallavi Iyer, Dr. Lyudmila Slipchenko, and Sarom Sok for all the helpful discussions.

The inspiration, encouragement, and help from my friends and colleagues, especially Gaurav Pranami. Dr. Rastko Sknepnek, Dr. Nicholas Suek, and Zhiju Zheng is greatly appreciated.

Special thanks to my parents and family. Their support, love, and encouragement made this accomplishment possible.